Common genetic variants in *CHRNA5* alter β-amyloid neuropathology and highlight chandelier cells in human aging and Alzheimer's disease

Jonas Rybnicek[1], Yuxiao Chen[2], Milos Millic[2], JoAnne McLaurin[3], Philip L De Jager[4], Julie A Schneider[5], Yanling Wang[6], David A Bennett[6], **Shreejoy Tripathy*[1, 2, 7, 8], Daniel Felsky*[2, 7, 8], Evelyn K Lambe*[1, 7, 9]**

1. Department of Physiology, University of Toronto, Toronto ON, Canada

2. Krembil Centre for Neuroinformatics, Centre for Addiction and Mental Health, Toronto ON, Canada

3. Biological Sciences, Sunnybrook Research Institute, Toronto, ON M4N 3M5, Canada.

4. Center for Translational & Computational Neuroimmunology, Department of Neurology and the Taub Institute for Research on Alzheimer's Disease and the Aging Brain, Columbia University Irving Medical Center, New York NY, USA

5. Department of Pathology, Rush University, Chicago IL, USA

6. Department of Neurological Sciences, Rush University, Chicago IL, USA

7. Department of Psychiatry, University of Toronto, Toronto ON, Canada

8. Institute of Medical Science, University of Toronto, Toronto ON, Canada

9. Department of OBGYN, University of Toronto, Toronto ON, Canada

*Co-corresponding authors

Co-Corresponding Authors email addresses:

Shreejoy Tripathy: shreejoy.tripathy@camh.ca

Dan Felsky: daniel.felsky@camh.ca

Evelyn Lambe: evelyn.lambe@utoronto.ca

Number of Pages: 25

Number of Figures: 7

Number of Tables: 1

Acknowledgements: This work was supported by the Canadian Institutes of Health Research (CIHR; MOP89825 and CIHR PJT-153101; EKL). DF is supported by the Krembil Foundation, Koerner Family Foundation, Canadian Institutes of Health Research, and the CAMH Discovery Fund. ST is supported by CAMH Discovery Fund, Krembil Foundation, Kavli Foundation, McLaughlin Foundation, Natural Sciences and Engineering Research Council of Canada (RGPIN-2020-05834 and DGECR-2020-00048), and Canadian Institutes of Health Research (NGN-171423). JM is supported by the Canadian Research Chairs program, as a Tier 1 Chair. ROSMAP is supported by P30AG10161, P30AG72975, R01AG15819, R01AG17917. U01AG46152, U01AG61356. ROSMAP resources can be requested at https://www.radc.rush.edu

Abstract

Changes in high-affinity nicotinic acetylcholine receptors are intricately connected to cognitive impairment in Alzheimer's Disease (AD). While preclinical work suggests a possible protective and cognitive-enhancing role for the auxiliary nicotinic α5 subunit, mRNA expression of the *CHRNA5* gene has not been closely examined in the context of human aging and dementia. Here, we investigate the impact of two common SNPs predicted to have different effects on the nicotinic α5 subunit: the function-compromising rs16969968 and the expression-altering rs1979905. We analyzed data from human prefrontal cortex (922 subjects with matched genotypic and *post-mortem* RNA sequencing, including 22 subjects with single-nucleus data) of elderly participants in the Religious Orders Study and Memory and Aging Project (ROS/MAP). We tested the impact of SNP haplotypes on prefrontal expression of *CHRNA5* as well as that of SNPs in its receptor partners: *CHRNA4* and *CHRNB2*. In the context of cognition and neuropathology, we observed a significant negative association between the high *CHRNA5*-expressing rs1979905A2 genotype and β-amyloid load in the prefrontal cortex. Our analyses revealed that the greatest abundance of *CHRNA5* expression was in chandelier neurons, a sparse but disproportionately-powerful set of interneurons, in addition to layer 5 and 6 pyramidal neurons. In subjects with functionally-unaltered *CHRNA5,* the proportion of chandelier cells in the prefrontal cortex shows resilience to β-amyloid load, but this resilience is diminished in subjects homozygous for the minor allele of the *CHRNA5* missense SNP rs16969968. Taken together, these findings urge further investigation into the role of *CHRNA5* and chandelier cells in AD neuroprotection.

Significance statement: The nicotinic α5 subunit is important for attention and cognition, however its relationship to aging and neuropathology is unknown. Our findings suggest that polymorphisms affecting *CHRNA5* expression associate with altered brain amyloid pathology. Cell type-specific expression of *CHRNA5* in the prefrontal cortex implicates chandelier interneurons as a focus of α5-mediated nicotinic signalling, potentially involved in regulating amyloid load. We find that a missense *CHRNA5* polymorphism is correlated with increased sensitivity of this class of interneuron to amyloid pathology. A neuroprotective role for *CHRNA5* identifies it as a possible target for therapies to improve neuron survival and excitatory/inhibitory balance in AD pathology.

Introduction

The cholinergic system plays a critical role in the pathology of Alzheimer's disease (AD) (Hampel et al., 2018), a neurodegenerative disease marked by the accumulation of β-amyloid peptide (β-amyloid) and neurofibrillary tangles of phosphorylated tau in the brain (Busche & Hyman, 2020). In AD, there are well characterized disturbances in the excitation/inhibition (E/I) balance in the cerebral cortex (Lauterborn et al., 2021; Vico Varela et al., 2019), arising from the disruption of inhibitory signalling (Garcia-Marin et al., 2009; León-Espinosa et al., 2012; Petrache et al., 2019). The shift toward higher excitation in the cortex is associated with cognitive impairment in AD (Noebels, 2011).

The cholinergic system is an important regulator of E/I balance in the prefrontal cortex (PFC) (Obermayer et al., 2019; Pafundo et al., 2013). In AD, there is a decrease of cortical nicotinic acetylcholine receptor binding (Court et al., 2001), and β-amyloid binding to nicotinic receptors has been postulated as a potential mediator of AD pathology (Buckingham et al., 2009; Lasala et al., 2019) possibly via blockade of these receptors (Lamb et al., 2005; Wu et al., 2004). By contrast, stimulation of nicotinic receptors has been found to improve neuronal survival in AD pathology (Kihara et al., 1997), promote neurogenesis, and improve cognition (He et al., 2013; Nie et al., 2013). Promoting nicotinic signalling using acetylcholinesterase inhibitors is one of the mainstay AD treatments (Deardorff et al., 2015).

The high-affinity nicotinic acetylcholine receptors are hetero-pentamer cation channels most commonly composed of α4 and β2 subunits (α4β2) (Albuquerque et al., 2009). Deep layer PFC pyramidal cells express nicotinic receptors also containing the auxiliary α5 subunit (Wada et al., 1990; Winzer-Serhan & Leslie, 2005). Nicotinic α5 subunits do not contribute to the acetylcholine binding site and cannot form functional receptors on their own (Ramirez-Latorre et al., 1996), requiring the binding sites provided by partner subunits α4 and β2, forming the α4β2α5 nicotinic receptor. The α5 subunit alters the kinetics of the nicotinic receptors (Venkatesan & Lambe, 2020) and increases their permeability to calcium ions (Scholze & Huck, 2020; Sciaccaluga et al., 2015). Furthermore, β-amyloid may bind less readily to the α4β2α5 than the α4β2 nicotinic receptor (Lamb et al., 2005), which raises the question of a possible protective role of the α5 subunit in AD pathology.

The α5 subunit has previously been linked to cognitive performance with loss of this nicotinic subunit resulting in worsened performance in attentional tasks in animal models (Bailey et al., 2010; Howe et al., 2018). In humans, single nucleotide polymorphisms (SNPs) affecting the expression and function of the *CHRNA5* gene, which codes for the α5 subunit, have been linked to attention and cognition deficits (Han et al., 2019; Schuch et al., 2016). These SNPs are also linked to smoking (Jensen et al., 2015), a major AD risk factor (Livingston et al., 2020). However, the involvement of *CHRNA5* in aging and Alzheimer's disease has not been studied.

We assessed the connections between SNPs affecting the expression and function of *CHRNA5*, and age-related cognitive and neuropathological phenotypes using detailed clinical and post-mortem data from the Religious Order Study and Memory and Aging Project (ROS/MAP) (Bennett et al., 2018). In particular, we tested the relationships among polymorphisms affecting *CHRNA5* expression (Smith et al., 2011) or function (Maskos, 2020) and AD pathology. Our findings suggest that people with higher levels of *CHRNA5* expression have lower β-amyloid accumulation. We find through single nucleus RNAseq analyses from Allen Institute and ROS/MAP databases that *CHRNA5* expression in humans is enriched in chandelier neurons, a subset of parvalbumin-expressing inhibitory neurons that exerts powerful and co-ordinated suppression of cortical excitation (Schneider-Mizell et al., 2021). Cell proportion analysis suggests that the missense SNP rs16969968 in *CHRNA5*, which alters the structure of the intracellular

loop of the α5 subunit and alters α5 function (Maskos, 2020), renders these important neurons more vulnerable to β-amyloid toxicity. Taken together, these results suggest a role for *CHRNA5* in maintaining the E/I balance in the forebrain and as a potential new target for therapies aiming to promote neuron survival in AD.

Methods

Study cohort

In our study we used data from 2004 deceased subjects from the ROS/MAP cohort study (Bennett et al., 2018), of whom 1732 were autopsied. Both studies enrolled subjects without known dementia. ROS enrolled elderly nuns and priests and MAP enrolled from community facilities and individual homes. Both studies were approved by an Institutional Review Board of Rush University Medical Center. Participants gave informed consent for annual clinical evaluation, signed an Anatomic Gift Act for brain donation at the time of death, and completed a repository consent allowing their resources to be shared. Most subjects assessed were female (68%) and all were non-Latino white. The average age at study entry was 80.5 ± 0.16 years and the average age at death was 89.2 ± 0.15 years. All data was retrieved from the Synapse AMP-AD Knowledge Portal (Synapse ID: syn2580853).

Selection of candidate single nucleotide polymorphisms (SNPs)

Nicotinic α5 subunits (encoded by *CHRNA5*) do not contribute to the acetylcholine binding site and cannot form functional receptors on their own (Ramirez-Latorre et al., 1996). In prefrontal cortex, the nicotinic α5 subunits participate in pentameric receptors with two binding sites contributed by partner subunits: α4 (encoded by *CHRNA4*) and β2 (encoded by *CHRNB2*) (Albuquerque et al., 2009). Together, these subunits form α4β2α5 nicotinic receptors (**Fig. 1**). While the current focus is *CHRNA5*, we also probed the impact of polymorphisms relevant to its receptor partners *CHRNA4* or *CHRNB2* for perspective. The specific polymorphisms were selected based on their reported effects on expression, coding, or clinical response. For *CHRNA5*, we selected the non-synonymous SNP rs16969968 in the coding region of *CHRNA5* and a cluster of 6 SNPs in linkage disequilibrium (LD) in the regulatory region of *CHRNA5* (Smith et al., 2011) represented here by rs1979905. These SNPs have previously been linked to altered *CHRNA5* expression (Smith et al., 2011) and altered risk of nicotine addiction (Jensen et al., 2015; Ji et al., 2015). For CHRNB2, the T allele of the rs2072660 polymorphism has previously been linked to altered risk for nicotine dependence (Wessel et al., 2010), and the T allele of the rs4292956 with a clinical response to treatment for smoking cessation (Swan et al., 2012). For *CHRNA4*, the G allele of the rs1044396 polymorphism has previously been associated with altered performance in attention tasks as well as with the regulation of *CHRNA4* expression (Sadaghiani et al., 2017).

Genotype data preparation and imputation

ROS/MAP participants were genotyped in two batches (Synapse ID: syn3219045): the first batch (n=1709) using the Affymetrix GeneChip 6.0 (Affymetrix, Inc, Santa Clara, CA, USA) at the Broad Institute's Center for Genotyping or the Translational Genomics Research Institute, and the second batch (n=382) using the Illumina HumanOmniExpress (Illumina, Inc, San Diego, CA, USA) at the Children's Hospital of Philadelphia. Both batches underwent the same initial quality control (QC) analysis, as described previously (De Jager et al., 2012). Only individuals with self-reported European ancestry were genotyped to minimize population heterogeneity. Sample-level quality control assessment included exclusion of samples with genotype success rate <95%, discordance between inferred and reported

gender, and excess heterozygosity. Imputation of genotype data was performed as described previously (Felsky et al., 2022). Each batch was imputed separately using the TOPMed Imputation Server (TOPMed reference r2), including Eagle (v2.4) for allelic phasing and Minimac4 (v1.5.7) for imputation. Prior to submission for imputation, genotypes were preprocessed using the TOPMed Imputation Server-recommended data preparation pipeline available here: https://topmedimpute.readthedocs.io/en/latest/prepare-your-data.html. Imputed output data from the TOPMed server for each batch were filtered for imputation quality (removing SNPs with r<0.8) before merging and mapping to rsIDs (dbSNP build 155). This resulted in a final high-quality dataset of 9,329,439 bi-allelic autosomal SNPs from 2061 individuals. Minor allele frequencies of candidate SNPs were calculated using the getmaf function of the BinaryDosage (1.0.0) R package.

Fine population structure

Principal component analysis (PCA) was performed on genotyped SNPs using PLINK2 (Purcell et al., 2007) to derive principal components representing fine population structure. The first 10 principal components were used as covariates in all linear regression models that included SNP or gene expression data.

Tissue preparation and bulk tissue RNA sequencing

Details on the preparation and handling of ROS/MAP post-mortem samples have been previously published (Jager et.al 2018). Samples were extracted using Qiagen's miRNeasy mini kit (cat. no. 217004) and the RNase free DNase Set (cat. no. 79254) and quantified by Nanodrop and quality was evaluated by Agilent Bioanalyzer. RNA sequencing on DLPFC tissue was carried out in 13 batches within three distinct library preparation and sequencing pipelines. Sequencing was carried out using the Illumina HiSeq (pipeline #1: 50M 101bp paired end reads) and NovaSeq6000 (pipeline #2: 30M 100bp paired end; pipeline #3: 40-50M 150bp paired end 121 reads). Full details on RNA extraction and sequencing are available on the Synapse AMP-AD 122 Knowledge Portal (syn3219045) and in Consens et al., 2022.

Processing of bulk DLPFC tissue RNAseq dataset

DLPFC RNAseq data processing, including gene expression residuals generation was performed as previously described (Felsky et al., 2022). In brief: All 13 DLPFC batches (ntotal = 1110) were processed using the same pipeline: 1) fastq file quality control was performed using FastQC v0.11.5 (default parameters), 2) STAR v2.5.3a was used to align reads (GRCh38.91 reference), 3) RSEM v1.2.31 was used to quantify expression from aligned BAM files, and 4) multiqc v1.5 was used to aggregate quality metrics from fastqc and Picard tools v2.17.4, 5) quality reports were examined for each batch and exclusion of samples was initially carried out according to manual identification of outlying samples primarily considering low numbers of aligned reads, excess GC coverage bias, high percentage of read duplicates, and abnormal distribution of read assignments across genomic annotations. Expression of the *XIST* gene was evaluated at this stage to exclude subjects with contradictory reported sex, 13 subjects were identified (new n total=1097).

DLPFC RNAseq data quality control

Full details of QC are available in Felsky et al. 2022. In brief: expected counts, calculated by RSEM, were aggregated, and used as input to limma (v3.48.3) voom in R (v4.1.1). Genes with insufficient expression (median count value was less than 15 across the combined sample) were removed. Naïve multidimensional scaling (MDS) analysis was then performed on the top 5000 most variable genes (using limma “plotMDS”) to identify subjects with outlying expression patterns. Outliers were defined as those with values of either of the first two latent dimensions exceeding ±4 times the interquartile range (IQR)

170 of their within-batch median value. Following this step, 1091 subjects remained for the DLPFC data.
171 These QC data were then trimmed mean of M-values (TMM) normalized.
172
173 ***Final QC and generation of gene expression residuals***
174
175 To ensure the robustness of included data, linear effects of identified technical co-variates, age at death
176 and post-mortem interval (PMI), and biological sex were removed using the "lmfit" (specifying robust
177 Huber regression (Huber, 2011), and expression values residualized. Individuals were then hierarchically
178 clustered (agglomerative) and the resulting dendrograms (Supplementary figure 9 of Felsky et al. 2022)
179 were manually inspected to identify any additional subject outliers escaping recognition by two-
180 dimensional MDS (18 identified). This resulted in a high-quality dataset of DLPFC bulk tissue (ngenes=17
181 465). The calculated gene expression residuals were used in all analyses assessing gene expression with
182 other variables in our study.

183 **Neuropathology and cognitive scores**

184 The ROS/MAP neuropathology data used in our study included measurements of average β-amyloid
185 peptide load and density of paired helical filament tau tangles across 8 brain regions (hippocampus,
186 entorhinal cortex, midfrontal cortex, inferior temporal cortex, angular gyrus, calcarine cortex, anterior
187 cingulate cortex, superior frontal cortex). Amyloid beta protein was identified by molecularly specific
188 immunohistochemistry and quantified by image analysis. Neuronal neurofibrillary tangles were identified
189 by molecularly specific immunohistochemistry (antibodies to abnormally phosphorylated Tau protein,
190 AT8). As recommended by the ROS/MAP study authors, the square-root of the averages of β-amyloid
191 load and tangle density was used in all analyses in our study. Post-mortem neuropathology data was
192 available from 1694 subjects.

193 The global cognition score was calculated at each visit as the average of 19 tests assessing the
194 subjects' episodic, working, and semantic memory, and perceptual orientation and speed. The raw score
195 of each test were converted to Z scores and averaged to yield a global cognition score. The z-scores have
196 a mean of 0 and standard deviation of 1. A negative z-score means that someone has a global cognition
197 score lower than the cohort average at baseline. We used only the global cognition score recorded at the
198 subject's last recorded session before death for our analysis. Global cognition scores at the last visit
199 before death were available from 1853 subjects.

200 **Smoking status**

201 The smoking status of the ROS/MAP participants was determined at the baseline interview by
202 participants' answers to the following questions: 1. "Do you smoke cigarettes now?"; 2. "Did you ever
203 smoke cigarettes regularly". Question 1 was used to determine current smokers, and question 2
204 identified former smokers. Participants who answered "no" to both questions were categorized as
205 "never smoked".

206 **Single-nucleus RNA sequencing and pre-processing**
207
208 Details on the nucleus isolation and single nucleus RNA sequencing from the dorsolateral prefrontal
209 cortex of 24 ROS/MAP subjects performed by Cain et al. 2020 are available on the Synapse AMP-AD
210 Knowledge Portal (ID: syn16780177) and in the Cain et al. 2020 preprint. In brief, nuclei from an
211 individual sample were loaded on a single channel on the 10x Genomics Chromium chip. Library
212 construction was then performed as per the Chromium Single Cell 3' Reagent Kit v2 protocol (CG00052)
213 provided by the manufacturer. The described protocol produces Illumina-ready sequencing libraries. All

214 sequencing was performed on an Illumina HiSeq4000 machine. Generation of count files from the raw
215 sequencing data was performed using the Cellranger software package (version 2.1.1, chemistry V2, 10X
216 Genomics, for chemistry Single Cell 3'). For every nucleus, the number of genes for which at least one
217 read was mapped was quantified, all nuclei with fewer than 400 detected genes were excluded.

218 **Single-nucleus RNA sequencing data processing**

219 The single-nucleus gene counts and metadata available from Cain et al. 2020 on synapse (ID:
220 syn16780177) were converted into a Seurat object (Satija et al., 2015) in R Studio for further processing.
221 Potential doublets were removed by filtering out cells with over 2500 detected features, and potential
222 dead or dying cells were removed by excluding cells expressing over 5% mitochondrial genes. Cell type
223 annotations were indicated in the data as described in the metadata downloaded from the Cain et al.
224 2020 Synapse repository (ID: syn16780177). The snRNAseq data was log-normalized and matched with
225 genotype data (n = 22 subjects). *CHRNA5* expression was averaged per cell type per individual and
226 *CHRNA5* levels in different cell types were then compared between cell types by one-way ANOVA with
227 Tuckey's post-hoc t-test. To prevent bias for rare cell types in calculating average *CHRNA5* expression per
228 cell type per individual, cell types with fewer than 100 individual cells represented in the original data
229 (not aggregated) were removed (the layer 5 FEZF2 ET cell type was excluded from analysis as only 93
230 cells of this type were present in the genotype-matched snRNAseq dataset).

231 **Estimates of relative cell type proportions from bulk DLPFC RNAseq**

232 Estimates of cell-type proportions from bulk DLPFC RNAseq data from 640 ROS/MAP participants was
233 performed and described by Cain et al. 2020. In brief: The authors developed a custom regression-based
234 consensus model, CelMod, to extract cell cluster specific genes from the snRNAseq dataset from 24
235 ROS/MAP participants, and then used these genes to estimate the proportions of different cell subtypes
236 in the bulk DLPFC RNAseq dataset from 640 ROS/MAP subjects. The deconvolved cell-type proportion
237 data from the DLPFC was available on request from the research group (Cain et al. 2020 personal
238 communication). We matched the cell type proportion data with genotype, bulk DLPFC RNAseq, and
239 neuropathology (brain levels of β-amyloid and tau) data (final n = 549 subjects). At the time of analysis
240 full cell-type annotations (like that in the snRNA-seq data) were only available for the different classes of
241 inhibitory neuron proportions. The proportions of Inh.5, a PVALB+/LHX6+/THSD7A+ cell type, were
242 determined (Cain et al. 2020 personal communication) to represent chandelier cell proportions in DLPFC.

243 **Statistical approaches**

244 ***EQTL and conditional eQTL analyses of candidate SNPs and CHRNA gene expression in DLPFC***

245 All analyses were performed in R (R version 4.0.2) (R Core Team, 2020) unless otherwise indicated. For
246 eQTL analyses (n = 924), linear regression was used to model batch- and technical covariate-corrected
247 gene expression residuals against SNP allele counts, co-varying for the first 10 genomic principal
248 components (fine population structure), biological sex, age at death, and PMI. Bonferroni correction was
249 applied across tests (6 cis-eQTL tests performed). To assess the effects of the *CHRNA5* haplotypes tagged
250 by rs16969968 and rs1979905 on *CHRNA5* expression we used a nested ANOVA analysis with Sidak's
251 post-hoc test for multiple comparisons in GraphPad Prism.

252 ***Association analysis between SNPs, gene expression, AD neuropathology, and cognition***

253 To map the multi-omic relationships between candidate SNPs (n_{SNPs}= 6), cholinergic receptor gene
254 expression (n_{genes}= 3), post-mortem AD-related neuropathologies ($n_{pathologies}$=2), and global cognitive

255 performance at the population level, we fit a series of independent linear models, maximizing sample
256 sizes for each combination of data types and including appropriate technical and biological covariates.
257 SNPs were modelled using additive allelic dosage coding (i.e., 0,1,2). For the associations of SNPs with β-
258 amyloid and tau pathology (n = 1317), sex, age at death, post-mortem interval (PMI) and the genomic
259 PCs were included as covariates. For the associations of SNPs with global cognitive performance at time
260 of death (n = 1448), sex, age at death, years of education and the first 10 genomic PCs were included as
261 covariates. To aid in the interpretation of SNP and gene expression effects in the context of co-occurring
262 neuropathologies and cognitive dysfunction, we also modelled the effects of amyloid and tau measures
263 on each other and on the last cognition score in our dataset (n = 1253); sex, age at death, PMI and years
264 of education were used as covariates. For the association of gene expression residuals with
265 neuropathology (n = 914), sex, age at death, and PMI were used as covariates. For global cognition at
266 time of death, we used a linear regression model of *CHRNA4, CHRNA5* or *CHNB2* against the last global
267 cognition score using matched cognition and neuropathology data (n = 887). Sex, age at death and years
268 of education were used as covariates.

269 In total, we fit 36 models. All two-sided *p*-values for terms of interest were corrected using the
270 false discovery rate (FDR) approach (Benjamini & Hochberg, 1995), with corrected $p_{FDR}<0.05$ considered
271 significant.

272 We used a Chi-square test in GraphPad Prism to study the association between *CHRNA5* SNPs
273 genotype and participant smoking status at baseline.

274 ***Network visualization of multi-omic mapping***

275 To integrate our multi-level association analyses and aid global interpretation, we constructed a network
276 plot summarizing relationships among the different data types analysed (**Fig. 2**). Network nodes
277 correspond to individual independent and dependent variables, and each edge represents an association
278 derived from one of the linear models described above.

279 ***Cross-correlation of cholinergic gene expression and network construction***

280 To assess the correlation of *CHRNA5* to other major cholinergic genes in the bulk DLPFC dataset, we
281 performed a series of Pearson-correlation analyses on the residualized expression of the different
282 cholinergic genes and used the resulting correlations to construct a correlation network (**Fig. 3**). Network
283 nodes correspond to the different cholinergic genes and the edges represent the size of the correlation
284 coefficient (r). Only correlations significant after adjustment for false discovery rate (56 comparisons) are
285 shown in the network graph.

286 ***Analysis of single-nucleus RNAseq data from DLPFC***

287 The single-nucleus RNAseq dataset published by Cain et al. 2020 contained cells clustered into 37
288 subtypes. As we were interested in genotypic effects on *CHRNA5* expression in neurons specifically, to
289 narrow the scope of the analysis, non-neuronal cell subsets (microglia : Micro.1 – Micro.6,
290 oligodendrocyte:Olig.1 – Olig.4, endothelial cells: Endo.1 – Endo.4, astrocyte cells: Astr.1 – Astr.5) were
291 grouped into cell-subtype categories (Microglia, Oligodendrocytes, Endothelial cells, Astrocytes) while
292 neuronal cells were kept in their subtypes (except the L5 RORB IT subtype which was formed by grouping
293 the Exc.Exc.RORB_L5_IT_1 and Exc.Exc.RORB_L5_IT_2 subtypes) as defined in Cain et al. 2020. Using the
294 aggregate function in R, the log-normalized DLPFC snRNAseq *CHRNA5* expression (n = 24) was averaged
295 per cell type (subtype) per individual (using the unique participant "projid" IDs) as follows:
296 [aggregate(*CHRNA5* ~ projid + subtype, data, mean)].

To assess the expression of *CHRNA5* across the different cell types, we used a one-way ANOVA with Tukey's post-hoc t-test on the *CHRNA5* expression previously averaged per cell type per individual.

To assess the association between the rs1979905 genotype and *CHRNA5* expression in the DLPFC snRNAseq data, we matched the *CHRNA5* expression data averaged per cell type per individual with genotype data (final = 22). We then used general linear models covaried for sex, age at death and PMI to assess the association between the rs1979905 genotype and *CHRNA5* expression in the different cell types.

Interaction modelling of neuropathology, CHRNA5 genotype, and bulk-estimated cell type proportions

To assess the association between amyloid and tau neuropathology, and chandelier cell proportions, we used a linear regression model of these variables covaried for sex, age at death and PMI. A linear regression model with the same covariates was also used to assess the association between *CHRNA5* expression and chandelier cell proportions. To test the association between rs1979905 and rs16969968 genotype with chandelier cell proportions, we used a linear regression model covaried for sex, age at death and post-mortem interval. Finally, we used a linear interaction model to test the association between genotype-neuropathology interaction on the proportion of chandelier cells, covaried for sex, age at death, post-mortem interval and the first 10 genomic PCs: [Cell proportion ~ Genotype * Neuropathology + sex + age at death + PMI + PC1 + … + PC10].

Results

Expression of α4β2α5 receptor component genes is affected by single nucleotide polymorphisms

CHRNA5 and its high-affinity nicotinic subunit partners *CHRNA4* and *CHRNB2,* are expressed in the human cortex, and assemble to form α4β2* nicotinic receptors (Albuquerque et al., 2009), where the auxiliary site denoted by the asterisk can be filled by α5 (**Fig 1A**). We first sought to identify brain expression quantitative trait loci (eQTL) effects of gene variants previously shown to influence *CHRNA5* expression (Smith et al., 2011) and α5 coding (Kuryatov et al., 2011; Sciaccaluga et al., 2015). We performed this analysis in bulk dorsolateral prefrontal cortex (DLPFC) tissue from 924 elderly study participants, nearly doubling the sample size of the available brain xQTL-serve resource (http://mostafavilab.stat.ubc.ca/xqtl/) which was developed from an earlier release of ROS/MAP data.

In agreement with previous work (Smith et al., 2011), these variants were in weak-moderate linkage disequilibrium in our European ancestry sample (r^2=0.34). Also consistent with existing data (Wang et al., 2013), we found that dosage of the A allele of the missense SNP rs16969968 (minor allele frequency (MAF) = 0.33) in the coding region of *CHRNA5* (**Fig 1B**) was associated with lower *CHRNA5* expression (t = -13.93 $p = 3.98*10^{-40}$). A different SNP cluster in the regulatory region upstream of *CHRNA5* (**Fig 1B**), denoted here by the A allele of the tag SNP rs1979905 (MAF = 0.43), was associated with higher *CHRNA5* expression (t= 27.87, $p = 5.94*10^{-124}$) (**Fig. 1C**). Analyses of the coding-SNP rs16969968 and the regulatory-SNP rs1979905 SNPs together (**Fig. 1D**) showed that *CHRNA5* expression is predominantly regulated by the regulatory-SNP rs1979905 rather than the coding-SNP, rs16969968, as all rs1979905 A allele non-carriers showed similar levels of *CHRNA5* mRNA regardless of the rs16969968 A allele (Nested one-way ANOVA: F(2) = 229.6; Šidák's post-hoc test for multiple comparisons: rs1979905 A1 vs. rs1979905 A0 $p = 8*10^{-6}$, rs1979905 A2 vs. rs1979905 A1 $p = 0.004$, rs1979905A2 vs rs1979905A0 $p = 4*10^{-6}$). This was also demonstrated using a conditional eQTL model, where the effect of rs16969968 A allele on *CHRNA5* expression was lost when co-varying for rs1979905 A allele (rs16969968A: t = -1.068,

339 p = 0.2815; rs1979905A: t = 21.931, $p = 6.140*10^{-86}$). No trans-eQTL effects were detected (**Fig. 1E**)
340 between either of these SNPs on the expression of the partner nicotinic subunit genes, *CHRNA4* and
341 *CHRNB2*.

342 The α5 subunit cannot form functional nicotinic receptors on its own and does not contribute to
343 the acetylcholine binding site. The presence of the major nicotinic subunits α4 and β2 is required for the
344 formation of the α5-containing α4β2α5 receptor. Because of this, we next assessed the impact of genetic
345 regulators of the other α4β2α5 nicotinic receptor subunit genes in this dataset, extending our eQTL
346 analyses to SNPs in *CHRNA4* and *CHRNB2* that are known to be associated with altered gene expression
347 or with known clinical effects (Sadaghiani et al., 2017) (Hoft et al., 2011; Swan et al., 2012). Without
348 exception, eQTL SNP effects for these genes were weaker than those of rs16969968 and rs1979905 for
349 *CHRNA5*: the T allele of *CHRNB2* intronic variant rs2072660 (MAF = 0.23) was associated with lower
350 *CHRNB2* expression (t = -5, $p = 7.05*10^{-7}$), and a similar association with *CHRNB2* expression was seen
351 with the T allele of the *CHRNB2* non-coding variant rs4292956 (MAF = 0.07) (t = -5.244, $p = 2.02*10^{-7}$)
352 (**Fig. 1E**). For *CHRNA4,* the G allele of missense variant rs1044396 (MAF = 0.45) in the coding region of
353 *CHRNA4* was associated with higher *CHRNA4* expression (t = 3.67, $p = 0.0003$). We also utilized the Gene
354 Query function of the xQTLServe online tool (DLPFC of 534 ROS/MAP participants) to identify the T allele
355 of the intronic variant rs45497800 as associated with decreased *CHRNA4* expression (t = -6.92, $p = 1.32 *$
356 10^{-11}). We then replicated this association in our larger cohort of 924 ROS/MAP subjects (MAF = 0.07) (t =
357 -4.57, $p = 5.54*10^{-6}$) (**Fig. 1E**). No trans-eQTL effects were detected of these SNPs on the other nicotinic
358 subunit genes (**Fig. 1E**). Further analysis was focused only on the cis-eQTL effects.

359 **A *CHRNA5* polymorphism is negatively associated with brain amyloid levels**

360 The ROS/MAP database includes a predominantly non-smoking population (2% of subjects were current
361 smokers at baseline assessment). As SNPs in *CHRNA5* have been previously been associated with altered
362 smoking risk (Jensen et al., 2015; Schuch et al., 2016), we first used a Chi-square test to investigate the
363 associations between the genotype for the *CHRNA5* SNPs and smoking status at baseline
364 (current/former/never smoked) but found no relationship (data not shown). Smoking status was not
365 used in further analysis.

366 As the functioning of the high affinity α4β2α5 nicotinic receptor has previously been shown to be
367 important in attentional and cognitive processing (Bailey et al., 2010; Howe et al., 2018), we performed a
368 series of linear regression analyses to assess the relationships between high-affinity nicotinic receptor
369 subunit SNP genotypes, post-mortem gene expression, β-amyloid and tau neuropathology, and
370 antemortem cognitive performance in the ROS/MAP dataset. As illustrated in **Fig. 2**, we found that the
371 expression of the major nicotinic subunit genes *CHRNA4* and *CHRNB2* showed positive associations with
372 the last global cognition score (*CHRNA4*: t = 2.98, p = 0.003; *CHRNB2*: t = 3.71, $p = 0.0002$). The
373 rs2072660 T allele, associated with lower *CHRNB2* expression, was negatively associated with the last
374 global cognition score (t = -2.14, $p = 0.032$). A similar negative association with the last global cognition
375 score (t = -2.46, $p = 0.014$) was found for the T allele of the *CHRNB2* SNP rs4292956, and this association
376 remained significant after false discovery rate (FDR) correction for multiple comparisons ($p_{FDR} = 0.039$).
377 Neither the rs1044396 G allele, which was positively associated with *CHRNA4* expression, nor the
378 rs45497800 T allele which showed a negative association with *CHRNA4* was associated with levels of
379 neuropathology or with the last global cognition score.

380 As expected, both β-amyloid and tau pathology were negatively associated with global cognitive
381 performance proximal to death (tau: t = -21 $p = 2.46*10^{-84}$; amyloid: t = -10.4, $p = -3.14*10^{-24}$) and
382 positively associated with each other (t = 17.68, $p = 6.96*10^{-63}$). While the *CHRNA5* expression was not
383 significantly associated with any of the metrics assessed, the A allele of the regulatory-SNP rs1979905,

384 which was positively associated with *CHRNA5* expression, was negatively associated with β-amyloid load
385 (t = -2.551, p = 0.011). This association remained significant after FDR correction (p_{FDR} = 0.032) but
386 showed no association with global cognition (data not shown). The A allele of the coding-SNP
387 rs16969968, which showed a significant negative association with *CHRNA5* expression, did not show a
388 significant association with neuropathology or global cognition (data not shown).

389 Considering the major role that the cholinergic system plays in AD pathology (Hampel et al.,
390 2018), it was surprising that only rs1979905, which influences the expression of the relatively sparsely
391 expressed *CHRNA5*, was significantly associated with AD-related neuropathology (β-amyloid) after
392 correction for multiple testing.

393 ***CHRNA5* expression does not tightly correlate with other components of the cholinergic system**

394 To investigate the interrelationships among *CHRNA5* and the major nicotinic subunits as well as other
395 components of the cholinergic system, we performed a series of expression correlation analyses. Most of
396 the major components of the cholinergic system which were detected in bulk DLPFC data of the
397 ROS/MAP subjects (*CHRNA2*, *CHRNA4*, *CHRNA7*, *CHRNB2*, *CHRM3*, *CHRM1* and *ACHE*) showed significant
398 positive correlation with each other (**Fig. 3**). By contrast, *CHRNA5* stood out as showing no positive
399 correlation with any of the other major cholinergic genes and only weak negative correlations with the
400 expression of *CHRNB2* and *CHRM1* (**Table 1**). Considering that the expression of *CHRNA5*, *CHRNB2,* and
401 *CHRNA4* are required for the assembly of the high-affinity α4β2α5 nicotinic receptor, it was surprising to
402 see that *CHRNA5* expression was not positively correlated with either *CHRNA4* or *CHRNB2* (**Fig. 3** and
403 **Table 1**). Therefore, we next investigated whether this lack of correlation may arise from differences in
404 the cell-type specific expression of *CHRNA5* compared to the major nicotinic receptor subunits, *CHRNA4*
405 and *CHRNB2,* which are more broadly expressed.

406 ***CHRNA5* shows stronger expression in chandelier interneurons than most other cell classes**

407 To assess the cell-type specificity of *CHRNA5* expression in the ROS/MAP cohort, we calculated the
408 average *CHRNA5* expression per cell type per individual using the genotype-matched single-nucleus
409 RNAseq data available from the DLPFC in a subset of 22 ROS/MAP participants (Cain et al., 2020)(2
410 subjects lacked genotyping data). In this small dataset, *CHRNA5* was expressed at a low level across a
411 number of different excitatory, inhibitory, and nonneuronal cell types (**Fig. 4A**), with significantly higher
412 expression in inhibitory PVALB+ chandelier cells (as identified by Cain et al. 2020). Chandelier cells had
413 significantly-higher expression of *CHRNA5* compared to most other cell types (One-way ANOVA: F(21) =
414 3.439, $p = 6.1*10^{-7}$; Tukey's post-hoc t-test Chandelier cells vs. 18 out of 19 other cell types: $p < 0.05$)
415 (**Fig. 4A**).

416 To investigate the cell type-specificity of the *CHRNA5* eQTL effects of the regulatory-SNP
417 rs1979905, we stratified the averaged *CHRNA5* expression by genotype for the rs1979905 A allele. We
418 found that higher allelic dosage of the rs1979905 A allele was associated with greater *CHRNA5*
419 expression (**Fig. 4B**), and that this pattern was most pronounced in subtypes of layer 5 (L5 RORB IT: t =
420 2.460, p = 0.0249) and layer 6 (L6 IT THEMIS: t = 2.402, p = 0.028) excitatory neurons (**Fig. 4C**). In PVALB+
421 chandelier cells, the additive effect was not significant (t = 0.554, p = 0.587). Other neuronal cell types
422 expressing *CHRNA5*, such as non-chandelier PVALB+ cells, appeared to diverge from the typical eQTL
423 pattern of rs1979905 (**Fig. 4C**). This analysis suggests that only a subset of *CHRNA5*-expressing cell-types
424 contribute to the stepwise expression pattern observed in the prefrontal cortex by rs1979905 genotype.
425 Chandelier cell expression of *CHRNA4* and *CHRNB2* were at a similar level to the expression levels of
426 these genes in many other cell types (**Fig. 5**).

To confirm the novel finding that chandelier cells show stronger *CHRNA5* expression compared to other classes of neurons, we probed publicly available cell-type specific gene expression databases of human brain tissue. Using the Allen Institute SMART-seq single-cell transcriptomics data from multiple cortical areas (https://celltypes.brain-map.org/rnaseq/human_ctx_smart-seq), we found *CHRNA5* expression to be highest in a PVALB+/SCUBE3+ inhibitory cell type (0.06 trimmed mean *CHRNA5* expression) likely representing chandelier cells (Hodge et al., 2019), and in a co-clustering PVALB+/MFI+ cell type (0.06 trimmed mean *CHRNA5* expression). In the Human Protein Atlas database (brain single cell tissue) (https://www.proteinatlas.org/ENSG00000169684-CHRNA5/single+cell+type/brain), *CHRNA5* showed highest expression in a PVALB+ inhibitory cell type (c-41) which also showed highest expression of *SCUBE3* (Inhibitory neurons c-41, 15.1 normalized *CHRNA5* transcripts per million), likely also representing chandelier cells.

The cell type specific data from ROS/MAP and the Allen database supports the hypothesis that *CHRNA5* possesses a distinctive expression pattern compared to its more abundant and widely-expressed subunit partners. In the context of the regulatory-SNP rs1979905, it appears that a subset of cell-types contributes disproportionately to the stepwise differences in *CHRNA5* expression observed in the prefrontal cortex.

A genotype-specific reduction in proportion of chandelier cells with increasing brain amyloid levels

To determine whether *CHRNA5* might promote chandelier neuron resilience to neurodegeneration, we examined the impact of AD neuropathology on estimated proportions of chandelier neurons in our bulk RNAseq dataset. Cell type proportion estimates for chandelier cells and several other interneuron subclasses were available, precomputed using sets of single-cell-informed marker genes, in a subset of 640 ROS/MAP participants (Cain et al., 2020). We found that β-amyloid levels were negatively associated with the proportion of chandelier cells ($t = -4.024$, $p = 7*10^{-5}$). While the proportion of chandelier cells did not differ outright by the regulatory-SNP rs1979905 or the coding-SNP rs16969968 genotype (data not shown), a significant negative association of the interaction of β-amyloid load and the rs16969968 A allele was observed with the proportion of chandelier cells in the DLPFC (**Fig. 6A**), with rs16969968 A allele homozygotes showing significantly lower chandelier cell proportions with increasing β-amyloid load, compared to rs16969968 A allele non-carriers (interaction term $t = -2.799$, $p = 0.005$). A near-significant positive association of rs1979905 A allele and β-amyloid levels with chandelier cells was also observed (**Fig. 6B**), with rs1979905 A allele homozygotes showing a trend towards a smaller drop in chandelier cell proportions with increasing β-amyloid, compared to rs1979905 A allele non-carriers (interaction term $t = 1.769$, $p = 0.078$). Chandelier cell proportions did not correlate with tau pathology ($t = -0.307$, $p = 0.759$), nor was there an interaction of *CHRNA5* genotype and tau pathology with chandelier cell proportions (data not shown).

To assess whether the interaction between β-amyloid levels and *CHRNA5* SNPs was driven by the effects of these SNPs on *CHRNA5* expression, we assessed the effect of the interaction of *CHRNA5* levels and β-amyloid load on chandelier cell proportion but found no significant effect ($t = 2.711$, $p = 0.544$). This suggests that the genotype-specific association between amyloid load and chandelier cell proportion is more likely driven by changes in nicotinic α5 protein structure and/or trafficking (Maskos, 2020) as a consequence of having two copies of the missense SNP in *CHRNA5*. The schematic in **Fig. 7** illustrates a working model of the impact of the rs16969968 A allele homozygosity for chandelier cell vulnerability.

469 Overall, our results suggest that SNPs regulating *CHRNA5* expression and function, may change
470 both the total β-amyloid levels in the brain and the susceptibility of specific *CHRNA5*-expressing cell
471 types to β-amyloid-mediated neurodegeneration.

472

473 **Discussion**

474 We examined human prefrontal cortical *CHRNA5* expression in aging, probing the connections between
475 SNPs affecting the expression and function of the nicotinic α5 subunit gene and AD-related
476 neuropathology. The aging prefrontal cortex demonstrates strong eQTL effects of the regulatory-SNP
477 rs1979905, and we show that the A allele of rs1979905 is associated with lower levels of brain β-
478 amyloid. Single-nucleus RNAseq data shows cell-type specificity of the eQTL effect, with subtypes of
479 layer 5 and layer 6 excitatory neurons contributing significant additive effects of the rs1979905 A allele
480 to *CHRNA5* expression. We discovered that PVALB+ chandelier cells show the greatest abundance of
481 *CHRNA5* in human prefrontal cortex. Lastly, we examined the impact of AD neuropathology on the
482 proportions of chandelier neurons and determined that the α5-altering coding-SNP rs16969968 renders
483 this interneuron population vulnerable to β-amyloid levels. Our findings suggest a potential cell-type
484 specific neuroprotective role for C*HRNA5* to reduce β-amyloid levels and toxicity.

485 *Inhibitory signalling is disrupted in Alzheimer's disease*

486 The disruption of the excitatory/inhibitory balance in the cortex is a hallmark of AD pathology and is
487 associated with cognitive AD symptoms (Lauterborn et al., 2021; Vico Varela et al., 2019). Previous
488 studies have shown disruption of cortical inhibitory signalling in AD stems in large part from the
489 alteration of both the activity of inhibitory neurons, as well as inhibitory cell loss (Hijazi et al., 2020;
490 Wright et al., 2013; Zheng et al., 2020). The susceptibility of inhibitory neurons to AD pathology is not
491 uniform, however. While studies have shown significant drops in somatostatin-positive interneurons in
492 the cortex of AD patients (Beal et al., 1986; Waller et al., 2020), the numbers of parvalbumin-positive
493 cortical interneurons, including the PVALB+ chandelier cells, appear more resilient to AD pathology
494 (Fonseca et al., 1993; Waller et al., 2020). Our study expands on these findings, demonstrating that the
495 preservation of chandelier cells in AD pathology depends on the genotype of the rs16969968 SNP. The
496 rs16969968 SNP is a missense mutation found to functionally alter the α5-containing nicotinic receptors
497 in cell systems and *in vivo*, through altered channel biosynthesis, trafficking, properties and/or
498 modulation (Forget et al., 2018; Koukouli et al., 2017; Kuryatov et al., 2011; Maskos, 2020; Sciaccaluga et
499 al., 2015). Recent optophysiological work suggests that the nicotinic α5 subunit accelerates the
500 endogenous cholinergic response in prefrontal cortex and protects it against desensitization (Venkatesan
501 & Lambe, 2020), but little is known about endogenous cholinergic modulation of chandelier neurons.

502 *Chandelier cells are vulnerable to β-amyloid pathology*

503 Chandelier cells are a specialized subtype of PVALB+ interneurons. They differ anatomically from the
504 PVALB+ basket cells by their large number of vertically oriented axonal cartridges, which specifically
505 innervate the axon initial segments of pyramidal neurons (Fairén & Valverde, 1980; Somogyi, 1977). New
506 evidence suggests a powerful role of the chandelier cells in regulating excitation dynamics of neuronal
507 networks (Schneider-Mizell et al., 2021). The chandelier cells have been proposed to be involved in
508 diseases involving pathological excitation in the cortex. In autism, where the cortical E/I balance is
509 disrupted leading to cognitive and social deficits (Pretzsch & Floris, 2020), chandelier cell numbers are
510 decreased (Amina et al., 2021). Similarly in epilepsy, which is typified by aberrant cortical excitation,

511 chandelier cell number are decreased (Ribak, 1985; Zhu et al., 2004). In contrast, in AD which is typified
512 by cortical E/I balance disruption (Lauterborn et al., 2021; Vico Varela et al., 2019), a previous study
513 found that while total number of chandelier cells in the cortex was not affected, the number of their
514 axonal cartridges was reduced (Fonseca et al., 1993). Furthermore, the inhibitory output of chandelier
515 cells has been previously found to be sensitive to β-amyloid pathology (León-Espinosa et al., 2012), but
516 unaffected by tau pathology (Blazquez-Llorca et al., 2010). Chandelier cell axons near β-amyloid plaques
517 have been found to show deformations, and pyramidal neurons proximal to plaques show loss of
518 inhibitory input onto their axon initial segments (León-Espinosa et al., 2012). Our findings suggest that in
519 people homozygous for A allele of the missense *CHRNA5* SNP rs16969968, this vulnerability of chandelier
520 cells to β-amyloid pathology may be exacerbated, possibly leading to cell death. Alternatively, because
521 the cortical cell-type proportions were estimated using patterns of marker gene expression (Cain et al.,
522 2020), the decreased chandelier cell proportions may be explained by the previously reported decrease
523 of chandelier cell cartridges in AD (Fonseca et al., 1993). It is possible that the rs16969968 A allele
524 homozygous genotype may lead to higher cartridge loss in AD, which may have resulted in lower
525 expression of chandelier-cell-specific marker genes in individuals with elevated β-amyloid.

526 *Potential mechanisms for a neuroprotective effect of α5-containing nicotinic receptors*

527 Our results suggest that polymorphisms affecting *CHRNA5* expression and function, may alter both the
528 total β-amyloid levels in the brain, and alter the susceptibility of specific *CHRNA5*-expressing cell types,
529 the chandelier cells, to β-amyloid-mediated toxicity. One possible explanation for these observations
530 may be the lowered binding of β-amyloid to the α4β2α5 nicotinic receptors (Lamb et al. 2005) expressed
531 by these cells. This protection against β-amyloid binding and inhibition of the nicotinic response (Wu et
532 al., 2004) could promote resilience of nicotinic signalling in the chandelier cells, potentially leading to
533 improved cell survival (Kihara et al., 1997) in AD pathology.
534 Furthermore, as α4β2α5 nicotinic receptors support higher conductance of calcium ions into the cell
535 (Scholze & Huck, 2020; Sciaccaluga et al., 2015), another putative neuroprotective mechanism of the α5
536 subunit may be through driving possible calcium-dependent pro-survival pathways in the neurons which
537 express the α4β2α5 nicotinic receptors (Cingir Koker et al., 2018; Ueda et al., 2008).

538 *Caveats and opportunities for additional investigation*

539 While the ROS/MAP database offered an opportunity to assess the impact of *CHRNA5* expression and
540 *CHRNA5*-related SNPs on AD pathology in a large sample, some caveats exist. As *CHRNA5* expression has
541 previously been shown to be important for animal performance in demanding attentional tasks (Bailey et
542 al., 2010; Howe et al., 2018), one of the critical limitations of our study is that a robust attention
543 assessment of the ROS/MAP subjects was not part of the study design, potentially explaining the lack of
544 any correlation between *CHRNA5* expression/polymorphisms and a cognitive readout. Additionally, while
545 the ROS/MAP dataset presented an opportunity to study the effects of rs16969968 on a background of
546 an unusually-low smoking prevalence (Cornelius et al., 2022), future work would benefit from inclusion
547 of a more diverse group of subjects with more robust assessment of smoking history. In terms of
548 approaches, RNA sequencing data has been previously found to not fully capture the protein-level
549 changes in AD brains, which were detectable through a proteomic analysis (Johnson et al., 2022). This
550 limitation should be considered when interpreting the findings of our study, in which we utilized bulk
551 and single-nucleus RNAseq from the prefrontal cortex. Lastly, A limitation of the single-nucleus RNA
552 sequencing data (Cain et al., 2020) was its relatively low number of subjects, limiting the robustness of
553 comparing the effects of rs1979905 on *CHRNA5* expression across the different cell types. It also did not

554 allow for a robust study of any cell-type specific effects of rs16969968 on *CHRNA5* expression, as the
555 subjects sampled only contained a single rs16969968 A allele homozygous individual, and so this analysis
556 was not performed. The low numbers of individuals in the single-nucleus cohort also prevented a
557 comparison between our findings from the estimated cell-type proportions in the bulk RNAseq data and
558 the actual proportions of different cell types present in the single-nucleus data. Future studies involving
559 more subjects with single-nucleus RNAseq data could extend our findings on the interaction association
560 of the rs16969968 genotype and β-amyloid with chandelier cell proportions.

561 *Summary and implications*

562 A growing body of work suggests that cortical excitability is perturbed early in Alzheimer's disease
563 through impairment of inhibitory interneurons (Hijazi et al., 2020; Petrache et al., 2019). *CHRNA5* is
564 positioned to modulate the overall excitability of the prefrontal cortex in two ways: through the
565 excitation of a population of deep layer cortical pyramidal neurons (Venkatesan & Lambe, 2020; Wada et
566 al., 1990; Winzer-Serhan & Leslie, 2005) that send projections throughout prefrontal cortex and, as
567 ascertained from our findings in this study, through the excitation of specific subsets of cortical
568 interneurons, the chandelier cells. Functional investigation of the circuits involving the *CHRNA5*-
569 expressing chandelier cells, will be necessary to further elucidate the role of *CHRNA5* in the regulation of
570 cortical excitation, attention and cognition, and Alzheimer's disease pathology.

571 Our findings suggest that *CHRNA5* is involved in Alzheimer's disease neuropathology. The A allele
572 of the *CHRNA5* regulatory-SNP rs1979905 is associated with higher expression of *CHRNA5* and is further
573 associated with reduced β-amyloid load in the brain. In parallel, the A allele of the missense SNP,
574 rs16969968, is associated with fewer chandelier cells in subjects with high β-amyloid levels, suggesting
575 that differences in the protein structure of *CHRNA5* contributes cellular resiliency to β-amyloid
576 pathology. This combination suggests two potential neuroprotective roles of *CHRNA5* in β-amyloid
577 pathology and makes *CHRNA5* a potential target for therapies aiming to improve neuron survival in
578 Alzheimer's disease.

579

580

581

582

583

584

585

586

587

588

589

590

591 **References**

592 Albuquerque, E. X., Pereira, E. F. R., Alkondon, M., & Rogers, S. W. (2009). Mammalian Nicotinic
593 Acetylcholine Receptors: From Structure to Function. *Physiological Reviews*, *89*(1), 73–120.
594 https://doi.org/10.1152/physrev.00015.2008

595 Amina, S., Falcone, C., Hong, T., Wolf-Ochoa, M. W., Vakilzadeh, G., Allen, E., Perez-Castro, R., Kargar, M.,
596 Noctor, S., & Martínez-Cerdeño, V. (2021). Chandelier Cartridge Density Is Reduced in the
597 Prefrontal Cortex in Autism. *Cerebral Cortex*, *31*(6), 2944–2951.
598 https://doi.org/10.1093/cercor/bhaa402

599 Bailey, C. D. C., De Biasi, M., Fletcher, P. J., & Lambe, E. K. (2010). The Nicotinic Acetylcholine Receptor
600 α5 Subunit Plays a Key Role in Attention Circuitry and Accuracy. *The Journal of Neuroscience*,
601 *30*(27), 9241 LP – 9252. https://doi.org/10.1523/JNEUROSCI.2258-10.2010

602 Beal, M. F., Mazurek, M. F., Svendsen, C. N., Bird, E. D., & Martin, J. B. (1986). Widespread reduction of
603 somatostatin-like immunoreactivity in the cerebral cortex in Alzheimer's disease. *Annals of*
604 *Neurology*, *20*(4), 489–495. https://doi.org/10.1002/ana.410200408

605 Benjamini, Y., & Hochberg, Y. (1995). Controlling the False Discovery Rate: A Practical and Powerful
606 Approach to Multiple Testing. *Journal of the Royal Statistical Society. Series B (Methodological)*,
607 *57*(1), 289–300. http://www.jstor.org/stable/2346101

608 Bennett, D. A., Buchman, A. S., Boyle, P. A., Barnes, L. L., Wilson, R. S., & Schneider, J. A. (2018). Religious
609 Orders Study and Rush Memory and Aging Project. *Journal of Alzheimer's Disease : JAD*, *64*(s1),
610 S161–S189. https://doi.org/10.3233/JAD-179939

611 Blazquez-Llorca, L., Garcia-Marin, V., & Defelipe, J. (2010). Pericellular innervation of neurons expressing
612 abnormally hyperphosphorylated tau in the hippocampal formation of Alzheimer's disease
613 patients. *Frontiers in Neuroanatomy*, *4*, 20. https://doi.org/10.3389/fnana.2010.00020

614 Buckingham, S. D., Jones, A. K., Brown, L. A., & Sattelle, D. B. (2009). Nicotinic acetylcholine receptor
615 signalling: roles in Alzheimer's disease and amyloid neuroprotection. *Pharmacological Reviews*,
616 *61*(1), 39–61. https://doi.org/10.1124/pr.108.000562

617 Busche, M. A., & Hyman, B. T. (2020). Synergy between amyloid-β and tau in Alzheimer's disease. *Nature*
618 *Neuroscience*, *23*(10), 1183–1193. https://doi.org/10.1038/s41593-020-0687-6

619 Cain, A., Taga, M., McCabe, C., Hekselman, I., White, C. C., Green, G., Rozenblatt-Rosen, O., Zhang, F.,
620 Yeger-Lotem, E., Bennett, D. A., Yang, H.-S., Regev, A., Menon, V., Habib, N., & De Jager, P. L.
621 (2020). Multi-cellular communities are perturbed in the aging human brain and with Alzheimer's
622 disease. *BioRxiv*. https://doi.org/10.1101/2020.12.22.424084

623 Cingir Koker, S., Jahja, E., Shehwana, H., Keskus, A. G., & Konu, O. (2018). Cholinergic Receptor Nicotinic
624 Alpha 5 (CHRNA5) RNAi is associated with cell cycle inhibition, apoptosis, DNA damage response
625 and drug sensitivity in breast cancer. *PloS One*, *13*(12), e0208982.
626 https://doi.org/10.1371/journal.pone.0208982

627 Consens, M. E., Chen, Y., Menon, V., Wang, Y., Schneider, J. A., De Jager, P. L., Bennett, D. A., Tripathy, S.
628 J., & Felsky, D. (2022). Bulk and Single-nucleus Transcriptomics Highlight Intra-telencephalic and
629 Somatostatin Neurons in Alzheimer's Disease. *BioRxiv*, 2022.01.12.476076.
630 https://doi.org/10.1101/2022.01.12.476076

631 Cornelius, M. E., Loretan, C. G., Wang, T. W., Jamal, A., & Moma, D. M. (2022). Tobacco Product Use

Among Adults — United States, 2020. *MMWR Morb Mortal Wkly Rep*, *71*, 397–405. https://doi.org/http://dx.doi.org/10.15585/mmwr.mm7111a1external icon

Court, J., Martin-Ruiz, C., Piggott, M., Spurden, D., Griffiths, M., & Perry, E. (2001). Nicotinic receptor abnormalities in Alzheimer's disease. *Biological Psychiatry*, *49*(3), 175–184. https://doi.org/https://doi.org/10.1016/S0006-3223(00)01116-1

De Jager, P. L., Shulman, J. M., Chibnik, L. B., Keenan, B. T., Raj, T., Wilson, R. S., Yu, L., Leurgans, S. E., Tran, D., Aubin, C., Anderson, C. D., Biffi, A., Corneveaux, J. J., Huentelman, M. J., Initiative, A. D. N., Rosand, J., Daly, M. J., Myers, A. J., Reiman, E. M., … Evans, D. A. (2012). A genome-wide scan for common variants affecting the rate of age-related cognitive decline. *Neurobiology of Aging*, *33*(5), 1017.e1-1017.e15. https://doi.org/10.1016/j.neurobiolaging.2011.09.033

Deardorff, W. J., Feen, E., & Grossberg, G. T. (2015). The Use of Cholinesterase Inhibitors Across All Stages of Alzheimer's Disease. *Drugs & Aging*, *32*(7), 537–547. https://doi.org/10.1007/s40266-015-0273-x

Fairén, A., & Valverde, F. (1980). A specialized type of neuron in the visual cortex of cat: a Golgi and electron microscope study of chandelier cells. *The Journal of Comparative Neurology*, *194*(4), 761–779. https://doi.org/10.1002/cne.901940405

Felsky, D., Klein, H.-U., Menon, V., Ma, Y., Wang, Y., Milic, M., Zhukovsky, P., Schneider, J., Bennett, D., & Jager, P. De. (2022). Human peripheral monocytes capture elements of the state of microglial activation in the brain. *Nature Portfolio*. https://doi.org/10.21203/rs.3.rs-1226021/v1

Fonseca, M., Soriano, E., Ferrer, I., Martinez, A., & Tun˜on, T. (1993). Chandelier cell axons identified by parvalbumin-immunoreactivity in the normal human temporal cortex and in Alzheimer's disease. *Neuroscience*, *55*(4), 1107–1116. https://doi.org/https://doi.org/10.1016/0306-4522(93)90324-9

Forget, B., Scholze, P., Langa, F., Morel, C., Pons, S., Mondoloni, S., Besson, M., Durand-de Cuttoli, R., Hay, A., Tricoire, L., Lambolez, B., Mourot, A., Faure, P., & Maskos, U. (2018). A Human Polymorphism in CHRNA5 Is Linked to Relapse to Nicotine Seeking in Transgenic Rats. *Current Biology*, *28*(20), 3244-3253.e7. https://doi.org/https://doi.org/10.1016/j.cub.2018.08.044

Garcia-Marin, V., Blazquez-Llorca, L., Rodriguez, J.-R., Boluda, S., Muntane, G., Ferrer, I., & DeFelipe, J. (2009). Diminished perisomatic GABAergic terminals on cortical neurons adjacent to amyloid plaques . In *Frontiers in Neuroanatomy* (Vol. 3). https://www.frontiersin.org/article/10.3389/neuro.05.028.2009

Hampel, H., Mesulam, M.-M., Cuello, A. C., Farlow, M. R., Giacobini, E., Grossberg, G. T., Khachaturian, A. S., Vergallo, A., Cavedo, E., Snyder, P. J., & Khachaturian, Z. S. (2018). The cholinergic system in the pathophysiology and treatment of Alzheimer's disease. *Brain : A Journal of Neurology*, *141*(7), 1917–1933. https://doi.org/10.1093/brain/awy132

Han, W., Zhang, T., Ni, T., Zhu, L., Liu, D., Chen, G., Lin, H., Chen, T., & Guan, F. (2019). Relationship of common variants in CHRNA5 with early-onset schizophrenia and executive function. *Schizophrenia Research*, *206*, 407–412. https://doi.org/10.1016/j.schres.2018.10.011

He, N., Wang, Z., Wang, Y., Shen, H., & Yin, M. (2013). ZY-1, A Novel Nicotinic Analog, Promotes Proliferation and Migration of Adult Hippocampal Neural Stem/Progenitor Cells. *Cellular and Molecular Neurobiology*, *33*(8), 1149–1157. https://doi.org/10.1007/s10571-013-9981-0

Hijazi, S., Heistek, T. S., Scheltens, P., Neumann, U., Shimshek, D. R., Mansvelder, H. D., Smit, A. B., & van Kesteren, R. E. (2020). Early restoration of parvalbumin interneuron activity prevents memory loss

and network hyperexcitability in a mouse model of Alzheimer's disease. *Molecular Psychiatry*, *25*(12), 3380–3398. https://doi.org/10.1038/s41380-019-0483-4

Hodge, R. D., Bakken, T. E., Miller, J. A., Smith, K. A., Barkan, E. R., Graybuck, L. T., Close, J. L., Long, B., Johansen, N., Penn, O., Yao, Z., Eggermont, J., Höllt, T., Levi, B. P., Shehata, S. I., Aevermann, B., Beller, A., Bertagnolli, D., Brouner, K., … Lein, E. S. (2019). Conserved cell types with divergent features in human versus mouse cortex. *Nature*, *573*(7772), 61–68. https://doi.org/10.1038/s41586-019-1506-7

Hoft, N. R., Stitzel, J. A., Hutchison, K. E., & Ehringer, M. A. (2011). CHRNB2 promoter region: association with subjective effects to nicotine and gene expression differences. *Genes, Brain, and Behavior*, *10*(2), 176–185. https://doi.org/10.1111/j.1601-183X.2010.00650.x

Howe, W. M., Brooks, J. L., Tierney, P. L., Pang, J., Rossi, A., Young, D., Dlugolenski, K., Guillmette, E., Roy, M., Hales, K., & Kozak, R. (2018). α5 nAChR modulation of the prefrontal cortex makes attention resilient. *Brain Structure & Function*, *223*(2), 1035–1047. https://doi.org/10.1007/s00429-017-1601-1

Huber, P. J. (2011). *Robust Statistics BT - International Encyclopedia of Statistical Science* (M. Lovric (ed.); pp. 1248–1251). Springer Berlin Heidelberg. https://doi.org/10.1007/978-3-642-04898-2_594

Jensen, K. P., DeVito, E. E., Herman, A. I., Valentine, G. W., Gelernter, J., & Sofuoglu, M. (2015). A CHRNA5 Smoking Risk Variant Decreases the Aversive Effects of Nicotine in Humans. *Neuropsychopharmacology : Official Publication of the American College of Neuropsychopharmacology*, *40*(12), 2813–2821. https://doi.org/10.1038/npp.2015.131

Ji, X., Gui, J., Han, Y., Brennan, P., Li, Y., McKay, J., Caporaso, N. E., Bertazzi, P. A., Landi, M. T., & Amos, C. I. (2015). The role of haplotype in 15q25.1 locus in lung cancer risk: results of scanning chromosome 15. *Carcinogenesis*, *36*(11), 1275–1283. https://doi.org/10.1093/carcin/bgv118

Johnson, E. C. B., Carter, E. K., Dammer, E. B., Duong, D. M., Gerasimov, E. S., Liu, Y., Liu, J., Betarbet, R., Ping, L., Yin, L., Serrano, G. E., Beach, T. G., Peng, J., De Jager, P. L., Haroutunian, V., Zhang, B., Gaiteri, C., Bennett, D. A., Gearing, M., … Seyfried, N. T. (2022). Large-scale deep multi-layer analysis of Alzheimer's disease brain reveals strong proteomic disease-related changes not observed at the RNA level. *Nature Neuroscience*, *25*(2), 213–225. https://doi.org/10.1038/s41593-021-00999-y

Kihara, T., Shimohama, S., Sawada, H., Kimura, J., Kume, T., Kochiyama, H., Maeda, T., & Akaike, A. (1997). Nicotinic receptor stimulation protects neurons against beta-amyloid toxicity. *Annals of Neurology*, *42*(2), 159–163. https://doi.org/10.1002/ana.410420205

Koukouli, F., Rooy, M., Tziotis, D., Sailor, K. A., O'Neill, H. C., Levenga, J., Witte, M., Nilges, M., Changeux, J.-P., Hoeffer, C. A., Stitzel, J. A., Gutkin, B. S., DiGregorio, D. A., & Maskos, U. (2017). Nicotine reverses hypofrontality in animal models of addiction and schizophrenia. *Nature Medicine*, *23*(3), 347–354. https://doi.org/10.1038/nm.4274

Kuryatov, A., Berrettini, W., & Lindstrom, J. (2011). Acetylcholine receptor (AChR) α5 subunit variant associated with risk for nicotine dependence and lung cancer reduces $(\alpha4\beta2)_2\alpha5$ AChR function. *Molecular Pharmacology*, *79*(1), 119–125. https://doi.org/10.1124/mol.110.066357

Lamb, P. W., Melton, M. A., & Yakel, J. L. (2005). Inhibition of neuronal nicotinic acetylcholine receptor channels expressed in Xenopus oocytes by beta-amyloid1-42 peptide. *Journal of Molecular Neuroscience : MN*, *27*(1), 13–21. https://doi.org/10.1385/JMN:27:1:013

716 Lasala, M., Fabiani, C., Corradi, J., Antollini, S., & Bouzat, C. (2019). Molecular Modulation of Human α7
717 Nicotinic Receptor by Amyloid-β Peptides. *Frontiers in Cellular Neuroscience*, *13*.
718 https://doi.org/10.3389/fncel.2019.00037

719 Lauterborn, J. C., Scaduto, P., Cox, C. D., Schulmann, A., Lynch, G., Gall, C. M., Keene, C. D., & Limon, A.
720 (2021). Increased excitatory to inhibitory synaptic ratio in parietal cortex samples from individuals
721 with Alzheimer's disease. *Nature Communications*, *12*(1), 2603. https://doi.org/10.1038/s41467-
722 021-22742-8

723 León-Espinosa, G., DeFelipe, J., & Muñoz, A. (2012). Effects of amyloid-β plaque proximity on the axon
724 initial segment of pyramidal cells. *Journal of Alzheimer's Disease : JAD*, *29*(4), 841–852.
725 https://doi.org/10.3233/JAD-2012-112036

726 Livingston, G., Huntley, J., Sommerlad, A., Ames, D., Ballard, C., Banerjee, S., Brayne, C., Burns, A., Cohen-
727 Mansfield, J., Cooper, C., Costafreda, S. G., Dias, A., Fox, N., Gitlin, L. N., Howard, R., Kales, H. C.,
728 Kivimäki, M., Larson, E. B., Ogunniyi, A., … Mukadam, N. (2020). Dementia prevention, intervention,
729 and care: 2020 report of the Lancet Commission. *The Lancet*, *396*(10248), 413–446.
730 https://doi.org/10.1016/S0140-6736(20)30367-6

731 Maskos, U. (2020). The nicotinic receptor alpha5 coding polymorphism rs16969968 as a major target in
732 disease: Functional dissection and remaining challenges. *Journal of Neurochemistry*, *154*(3), 241–
733 250. https://doi.org/https://doi.org/10.1111/jnc.14989

734 Nie, H., Wang, Z., Zhao, W., Lu, J., Zhang, C., Lok, K., Wang, Y., Shen, H., Xu, Z., & Yin, M. (2013). New
735 nicotinic analogue ZY-1 enhances cognitive functions in a transgenic mice model of Alzheimer's
736 disease. *Neuroscience Letters*, *537*, 29–34.
737 https://doi.org/https://doi.org/10.1016/j.neulet.2013.01.001

738 Noebels, J. (2011). A perfect storm: Converging paths of epilepsy and Alzheimer's dementia intersect in
739 the hippocampal formation. *Epilepsia*, *52 Suppl 1*(Suppl 1), 39–46. https://doi.org/10.1111/j.1528-
740 1167.2010.02909.x

741 Obermayer, J., Luchicchi, A., Heistek, T. S., de Kloet, S. F., Terra, H., Bruinsma, B., Mnie-Filali, O.,
742 Kortleven, C., Galakhova, A. A., Khalil, A. J., Kroon, T., Jonker, A. J., de Haan, R., van de Berg, W. D.
743 J., Goriounova, N. A., de Kock, C. P. J., Pattij, T., & Mansvelder, H. D. (2019). Prefrontal cortical
744 ChAT-VIP interneurons provide local excitation by cholinergic synaptic transmission and control
745 attention. *Nature Communications*, *10*(1), 5280. https://doi.org/10.1038/s41467-019-13244-9

746 Pafundo, D. E., Miyamae, T., Lewis, D. A., & Gonzalez-Burgos, G. (2013). Cholinergic modulation of
747 neuronal excitability and recurrent excitation-inhibition in prefrontal cortex circuits: implications
748 for gamma oscillations. *The Journal of Physiology*, *591*(19), 4725–4748.
749 https://doi.org/10.1113/jphysiol.2013.253823

750 Petrache, A. L., Rajulawalla, A., Shi, A., Wetzel, A., Saito, T., Saido, T. C., Harvey, K., & Ali, A. B. (2019).
751 Aberrant Excitatory-Inhibitory Synaptic Mechanisms in Entorhinal Cortex Microcircuits During the
752 Pathogenesis of Alzheimer's Disease. *Cerebral Cortex (New York, N.Y. : 1991)*, *29*(4), 1834–1850.
753 https://doi.org/10.1093/cercor/bhz016

754 Pretzsch, C. M., & Floris, D. L. (2020). Balancing excitation and inhibition in the autistic brain. *ELife*, *9*,
755 e60584. https://doi.org/10.7554/eLife.60584

756 Purcell, S., Neale, B., Todd-Brown, K., Thomas, L., Ferreira, M. A. R., Bender, D., Maller, J., Sklar, P., de
757 Bakker, P. I. W., Daly, M. J., & Sham, P. C. (2007). PLINK: a tool set for whole-genome association

and population-based linkage analyses. *American Journal of Human Genetics*, *81*(3), 559–575. https://doi.org/10.1086/519795

Ramirez-Latorre, J., Yu, C. R., Qu, X., Perin, F., Karlin, A., & Role, L. (1996). Functional contributions of α5 subunit to neuronal acetylcholine receptor channels. *Nature*, *380*(6572), 347–351. https://doi.org/10.1038/380347a0

Ribak, C. E. (1985). Axon terminals of GABAergic chandelier cells are lost at epileptic foci. *Brain Research*, *326*(2), 251–260. https://doi.org/https://doi.org/10.1016/0006-8993(85)90034-4

Sadaghiani, S., Ng, B., Altmann, A., Poline, J.-B., Banaschewski, T., Bokde, A. L. W., Bromberg, U., Büchel, C., Burke Quinlan, E., Conrod, P., Desrivières, S., Flor, H., Frouin, V., Garavan, H., Gowland, P., Gallinat, J., Heinz, A., Ittermann, B., Martinot, J.-L., … Greicius, M. (2017). Overdominant Effect of a CHRNA4 Polymorphism on Cingulo-Opercular Network Activity and Cognitive Control. *Journal of Neuroscience*, *37*(40), 9657–9666. https://doi.org/10.1523/JNEUROSCI.0991-17.2017

Satija, R., Farrell, J. A., Gennert, D., Schier, A. F., & Regev, A. (2015). Spatial reconstruction of single-cell gene expression data. *Nature Biotechnology*, *33*(5), 495–502. https://doi.org/10.1038/nbt.3192

Schneider-Mizell, C. M., Bodor, A. L., Collman, F., Brittain, D., Bleckert, A., Dorkenwald, S., Turner, N. L., Macrina, T., Lee, K., Lu, R., Wu, J., Zhuang, J., Nandi, A., Hu, B., Buchanan, J., Takeno, M. M., Torres, R., Mahalingam, G., Bumbarger, D. J., … Costa, N. M. da. (2021). Structure and function of axo-axonic inhibition. *ELife*, *10*, e73783. https://doi.org/10.7554/eLife.73783

Scholze, P., & Huck, S. (2020). The α5 Nicotinic Acetylcholine Receptor Subunit Differentially Modulates α4β2* and α3β4* Receptors. *Frontiers in Synaptic Neuroscience*, *12*. https://doi.org/10.3389/fnsyn.2020.607959

Schuch, J. B., Polina, E. R., Rovaris, D. L., Kappel, D. B., Mota, N. R., Cupertino, R. B., Silva, K. L., Guimarães-da-Silva, P. O., Karam, R. G., Salgado, C. A. I., White, M. J., Rohde, L. A., Grevet, E. H., & Bau, C. H. D. (2016). Pleiotropic effects of Chr15q25 nicotinic gene cluster and the relationship between smoking, cognition and ADHD. *Journal of Psychiatric Research*, *80*, 73–78. https://doi.org/10.1016/j.jpsychires.2016.06.002

Sciaccaluga, M., Monconi, C., Martinello, K., Catalano, M., Bermudez, I., Stitzel, J. A., Maskos, U., & Fucile, S. (2015). Crucial role of nicotinic α5 subunit variants for Ca2+ fluxes in ventral midbrain neurons. *The FASEB Journal*, *29*(8), 3389–3398. https://doi.org/https://doi.org/10.1096/fj.14-268102

Smith, R. M., Alachkar, H., Papp, A. C., Wang, D., Mash, D. C., Wang, J.-C., Bierut, L. J., & Sadee, W. (2011). Nicotinic α5 receptor subunit mRNA expression is associated with distant 5' upstream polymorphisms. *European Journal of Human Genetics*, *19*(1), 76–83. https://doi.org/10.1038/ejhg.2010.120

Somogyi, P. (1977). A specific "axo-axonal" interneuron in the visual cortex of the rat. *Brain Research*, *136*(2), 345–350. https://doi.org/10.1016/0006-8993(77)90808-3

Swan, G. E., Javitz, H. S., Jack, L. M., Wessel, J., Michel, M., Hinds, D. A., Stokowksi, R. P., McClure, J. B., Catz, S. L., Richards, J., Zbikowski, S. M., Deprey, M., McAfee, T., Conti, D. V, & Bergen, A. W. (2012). Varenicline for smoking cessation: nausea severity and variation in nicotinic receptor genes. *The Pharmacogenomics Journal*, *12*(4), 349–358. https://doi.org/10.1038/tpj.2011.19

Ueda, M., Iida, Y., Kitamura, Y., Kawashima, H., Ogawa, M., Magata, Y., & Saji, H. (2008). 5-Iodo-A-85380, a specific ligand for alpha 4 beta 2 nicotinic acetylcholine receptors, prevents glutamate

neurotoxicity in rat cortical cultured neurons. *Brain Research*, *1199*, 46–52. https://doi.org/10.1016/j.brainres.2007.10.107

Venkatesan, S., & Lambe, E. K. (2020). Chrna5 is essential for a rapid and protected response to optogenetic release of endogenous acetylcholine in prefrontal cortex. *The Journal of Neuroscience*, *40*(38). https://doi.org/10.1101/2020.05.10.087569

Vico Varela, E., Etter, G., & Williams, S. (2019). Excitatory-inhibitory imbalance in Alzheimer's disease and therapeutic significance. *Neurobiology of Disease*, *127*, 605–615. https://doi.org/https://doi.org/10.1016/j.nbd.2019.04.010

Wada, E., McKinnon, D., Heinemann, S., Patrick, J., & Swanson, L. W. (1990). The distribution of mRNA encoded by a new member of the neuronal nicotinic acetylcholine receptor gene family (alpha 5) in the rat central nervous system. *Brain Research*, *526*(1), 45–53. https://doi.org/10.1016/0006-8993(90)90248-a

Waller, R., Mandeya, M., Viney, E., Simpson, J. E., & Wharton, S. B. (2020). Histological characterization of interneurons in Alzheimer's disease reveals a loss of somatostatin interneurons in the temporal cortex. *Neuropathology : Official Journal of the Japanese Society of Neuropathology*, *40*(4), 336–346. https://doi.org/10.1111/neup.12649

Wang, J.-C., Spiegel, N., Bertelsen, S., Le, N., McKenna, N., Budde, J. P., Harari, O., Kapoor, M., Brooks, A., Hancock, D., Tischfield, J., Foroud, T., Bierut, L. J., Steinbach, J. H., Edenberg, H. J., Traynor, B. J., & Goate, A. M. (2013). Cis-Regulatory Variants Affect CHRNA5 mRNA Expression in Populations of African and European Ancestry. *PLOS ONE*, *8*(11), e80204. https://doi.org/10.1371/journal.pone.0080204

Wessel, J., McDonald, S. M., Hinds, D. A., Stokowski, R. P., Javitz, H. S., Kennemer, M., Krasnow, R., Dirks, W., Hardin, J., Pitts, S. J., Michel, M., Jack, L., Ballinger, D. G., McClure, J. B., Swan, G. E., & Bergen, A. W. (2010). Resequencing of nicotinic acetylcholine receptor genes and association of common and rare variants with the Fagerström test for nicotine dependence. *Neuropsychopharmacology : Official Publication of the American College of Neuropsychopharmacology*, *35*(12), 2392–2402. https://doi.org/10.1038/npp.2010.120

Winzer-Serhan, U. H., & Leslie, F. M. (2005). Expression of alpha5 nicotinic acetylcholine receptor subunit mRNA during hippocampal and cortical development. *The Journal of Comparative Neurology*, *481*(1), 19–30. https://doi.org/10.1002/cne.20357

Wright, A. L., Zinn, R., Hohensinn, B., Konen, L. M., Beynon, S. B., Tan, R. P., Clark, I. A., Abdipranoto, A., & Vissel, B. (2013). Neuroinflammation and neuronal loss precede Aβ plaque deposition in the hAPP-J20 mouse model of Alzheimer's disease. *PloS One*, *8*(4), e59586. https://doi.org/10.1371/journal.pone.0059586

Wu, J., Kuo, Y.-P., George, A. A., Xu, L., Hu, J., & Lukas, R. J. (2004). beta-Amyloid directly inhibits human alpha4beta2-nicotinic acetylcholine receptors heterologously expressed in human SH-EP1 cells. *The Journal of Biological Chemistry*, *279*(36), 37842–37851. https://doi.org/10.1074/jbc.M400335200

Zheng, J., Li, H.-L., Tian, N., Liu, F., Wang, L., Yin, Y., Yue, L., Ma, L., Wan, Y., & Wang, J.-Z. (2020). Interneuron Accumulation of Phosphorylated tau Impairs Adult Hippocampal Neurogenesis by Suppressing GABAergic Transmission. *Cell Stem Cell*, *26*(3), 331-345.e6. https://doi.org/10.1016/j.stem.2019.12.015

Zhu, Y., Stornetta, R. L., & Zhu, J. J. (2004). Chandelier Cells Control Excessive Cortical Excitation: Characteristics of Whisker-Evoked Synaptic Responses of Layer 2/3 Nonpyramidal and Pyramidal Neurons. *The Journal of Neuroscience*, *24*(22), 5101 LP – 5108. https://doi.org/10.1523/JNEUROSCI.0544-04.2004

848 **Figure legends**

849 **Figure 1. Prefrontal α4β2* nicotinic acetylcholine receptor configurations and eQTL effects of SNPs on**
850 **nicotinic receptor subunit gene expression.** ***A,*** Schematics illustrating different subunit compositions of
851 prefrontal α4β2* nicotinic receptors, with and without the α5 subunit. ***B,*** Localization of the rs16969968
852 and rs1979905 SNPs in relation to the *CHRNA5* locus. ***C,*** The A allele of the missense SNP rs16969968
853 (left) in the coding region of *CHRNA5* is associated with lowered *CHRNA5* expression, while the A allele of
854 the rs1979905 SNP (middle) upstream of the *CHRNA5* gene is associated with enhanced *CHRNA5*
855 expression. Data from the DLPFC of ROS/MAP subjects. ***D,*** *CHRNA5* expression appears to be controlled
856 by the zygosity of the rs1979905 A allele (colors) instead of the rs16969968 A allele (x-axis). Data shown
857 as *CHRNA5* expression for each subject with means indicated. ***E,*** eQTL effects of SNPs in nicotinic subunit
858 genes on their respective gene expression. Shown as β-coefficient with significance (p) in brackets.

859 **Figure 2. Network modelling of the relationships among high-affinity nicotinic receptor subunits, their**
860 **SNPs, and phenotypic data.** Network plot depicting the relationships between SNPs (black), gene
861 expression (red), neuropathology (blue), and global cognition score (green). Only associations $p < 0.05$
862 before adjustment for false discovery rate (FDR) are indicated in the plot. Solid and dashed lines indicate
863 whether association was significant after correction for FDR or not, respectively.

864 **Figure 3. There is a tight interrelationship among the prefrontal expression of most cholinergic**
865 **receptor genes, which unexpectedly does not extend to the a5 subunit.** Network plot depicting the
866 correlations present between the expression of select cholinergic genes, colour of lines indicated
867 direction of correlation (negative or positive) while the thickness indicates correlation strength. While
868 the two major nicotinic subunits *CHRNA4* and *CHRNB2* are strongly positively correlated with other
869 components of the cholinergic system, the auxiliary subunit *CHRNA5* shows no positive correlation with
870 any of the cholinergic genes assessed. All correlations shown are significant after adjustment for false
871 discovery rate.

872 **Figure 4. *CHRNA5* expression is elevated in chandelier cells and is affected by genotype for the**
873 **rs1979905 A allele.** ***A,*** Expression of *CHRNA5* averaged per cell type per individual, original gene count
874 values were normalized for each cell by total expression. F-test significance of ANOVA shown on graph,
875 with red asterisk denoting post-hoc tests demonstrating *CHRNA5* expression is stronger in chandelier
876 cells compared to all but one other cell type. Mean expression of *CHRNA5* in chandelier cells displayed
877 (red line). ***B,*** Expression of *CHRNA5* across cell types in the PFC in subjects split by genotype for the
878 rs1979905 A allele, expression averaged per cell type per individual. Number of subjects per rs1979905 A
879 allele genotype: 0, n = 5; 1, n = 13; 2, n = 4. ***C,*** Effect of genotype for rs1979905 A allele on expression of
880 *CHRNA5* in selected cell types, data shown as *CHRNA5* expression averaged per cell type per individual. A
881 pattern of increasing *CHRNA5* expression with increasing rs1979905 A zygosity is present in some cell
882 types. Significance shown for linear regression models for L5 and L6 excitatory neurons. Displayed as
883 mean + SEM. Number of cells per subtype indicated (n_{cell}).

884 **Figure 5. *CHRNA4* and *CHRNB2* expression in chandelier cells and other prefrontal cell types.** The two
885 major high-affinity nicotinic subunit genes *CHRNA4* and *CHRNB2* are expressed in chandelier neurons,
886 but not disproportionately to their expression in the other neuronal cell types found in the snRNAseq
887 DLPFC dataset. ***A,*** Expression of *CHRNA4* across different cell types in the ROS/MAP DLPFC snRNAseq
888 dataset. Mean expression of *CHRNA4* in chandelier cells displayed (red line) ***B,*** Expression of *CHRNB2*
889 across different cell types in the ROS/MAP DLPFC snRNAseq dataset. Mean expression of *CHRNB2* in

890 chandelier cells displayed (red line)**.** Data shown as mean + SEM of the data averaged per cell-type per
891 individual.

892 **Figure 6. Association of chandelier cell proportions with β-amyloid load is dependent on the**
893 **rs16969968 A allele genotype**. ***A,*** Stratifying by rs16969968 A allele reveals a significant interaction
894 effect between rs16969968 A allele and amyloid load on chandelier cell proportions with rs16969968 A
895 allele homozygotes showing a significantly stronger association between brain amyloid load and
896 chandelier cell proportions compared to rs16969968 A allele non-carriers (t = -2.799, *p* = 0.005) ***B,***
897 Stratifying by rs1979905 A allele reveals a near significant interaction effect between rs1979905 A allele
898 and amyloid load on chandelier cell proportions with rs1979905 A allele homozygotes showing a less
899 negative association between brain amyloid load and chandelier cell proportions compared to rs1979905
900 A allele non-carriers (t = 1.769, *p* = 0.078). Scatter plots show 95% confidence intervals of linear model
901 predictions, β-coefficients and *p* values of individual linear regression models are displayed.

902 **Figure 7. A working model of the impact of *CHRNA5* genotype for chandelier cell (ChC) resilience and**
903 **vulnerability.** In coding-SNP rs16969968 non-carriers, the α4β2α5 nicotinic receptor is resistant to
904 inhibition by β-amyloid, preserving nicotinic signalling even at high β-amyloid levels that inhibit the α4β2
905 receptors. In coding-SNP rs16969968 homozygous subjects, the disruption of the α5 subunit may reduce
906 its representation in the receptors or block its protective function against β-amyloid, leading to disrupted
907 nicotinic signalling at higher β-amyloid levels, possibly triggering a cytotoxic response in the chandelier
908 cells.

Table 1. Expression correlation of selected cholinergic genes.

Results of Pearson's correlation analysis of the expression of selected cholinergic genes using the bulk tissue RNAseq data from the DLPFC of ROS/MAP subjects.

Gene 1	Gene 2	r	p	FDR
CHRNA4	*ACHE*	0.556	<0.001	<0.001
	CHRM1	0.542	<0.001	<0.001
	CHRM3	0.242	<0.001	0.002
	CHRNA2	0.307	<0.001	<0.001
	CHRNA7	0.131	0.039	0.464
	CHRNB2	0.457	<0.001	<0.001
CHRNA5	*ACHE*	0.063	0.324	1.000
	CHRM1	-0.309	<0.001	<0.001
	CHRM3	-0.095	0.134	1.000
	CHRNA2	-0.045	0.477	1.000
	CHRNA4	-0.130	0.041	0.464
	CHRNA7	-0.061	0.342	1.000
	CHRNB2	-0.248	<0.001	0.001
CHRNB2	*ACHE*	0.472	<0.001	<0.001
	CHRM1	0.846	<0.001	<0.001
	CHRM3	0.645	<0.001	<0.001
	CHRNA2	0.283	<0.001	<0.001
	CHRNA4	0.457	<0.001	<0.001
	CHRNA7	0.359	<0.001	<0.001

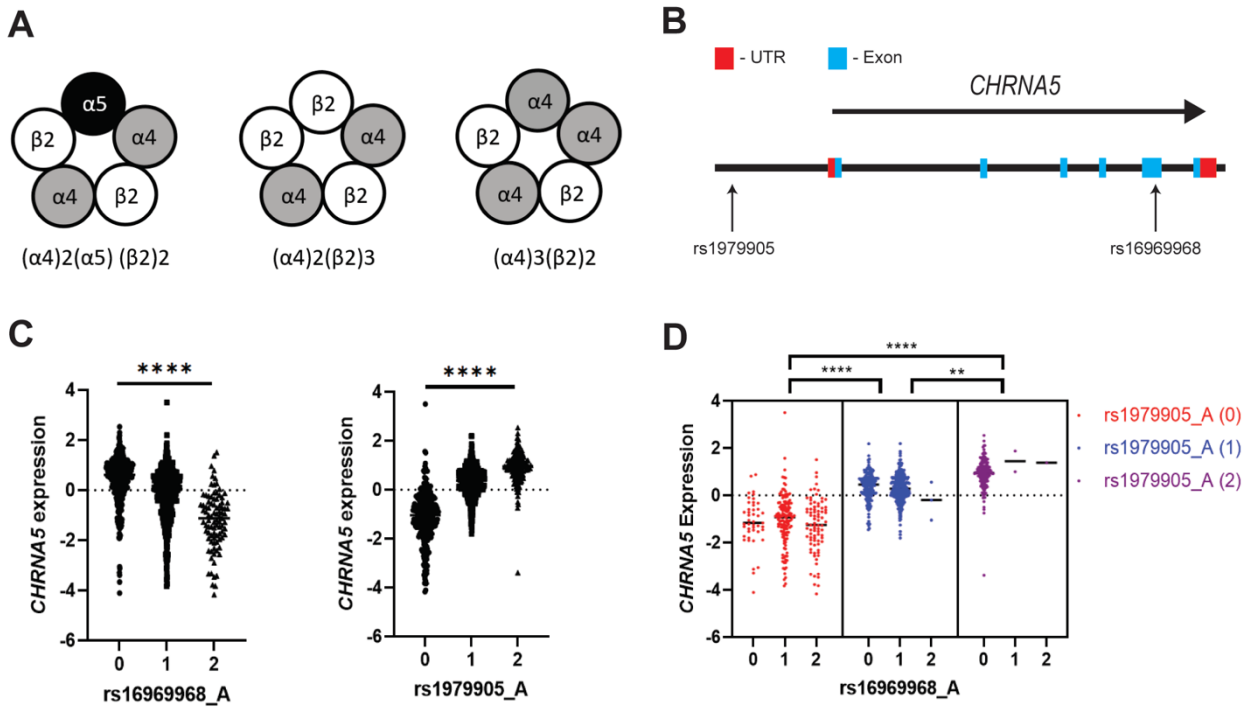

E

SNP/Gene	*CHRNA5*	*CHRNA4*	*CHRNB2*
rs1979905_A	1.083 ($5.94*10^{-124}$)	-	-
rs16969968_A	-0.713 ($3.98*10^{-40}$)	-	-
rs1044396_G	-	0.075 (0.0003)	-
rs4549700_T	-	-0.181 ($1.32 * 10^{-11}$)	-
rs4292956_T	-	-	-0.209 ($2.02*10^{-7}$)
rs2072660_T	-	-	-0.128 ($7.05*10^{-7}$)

Figure 1

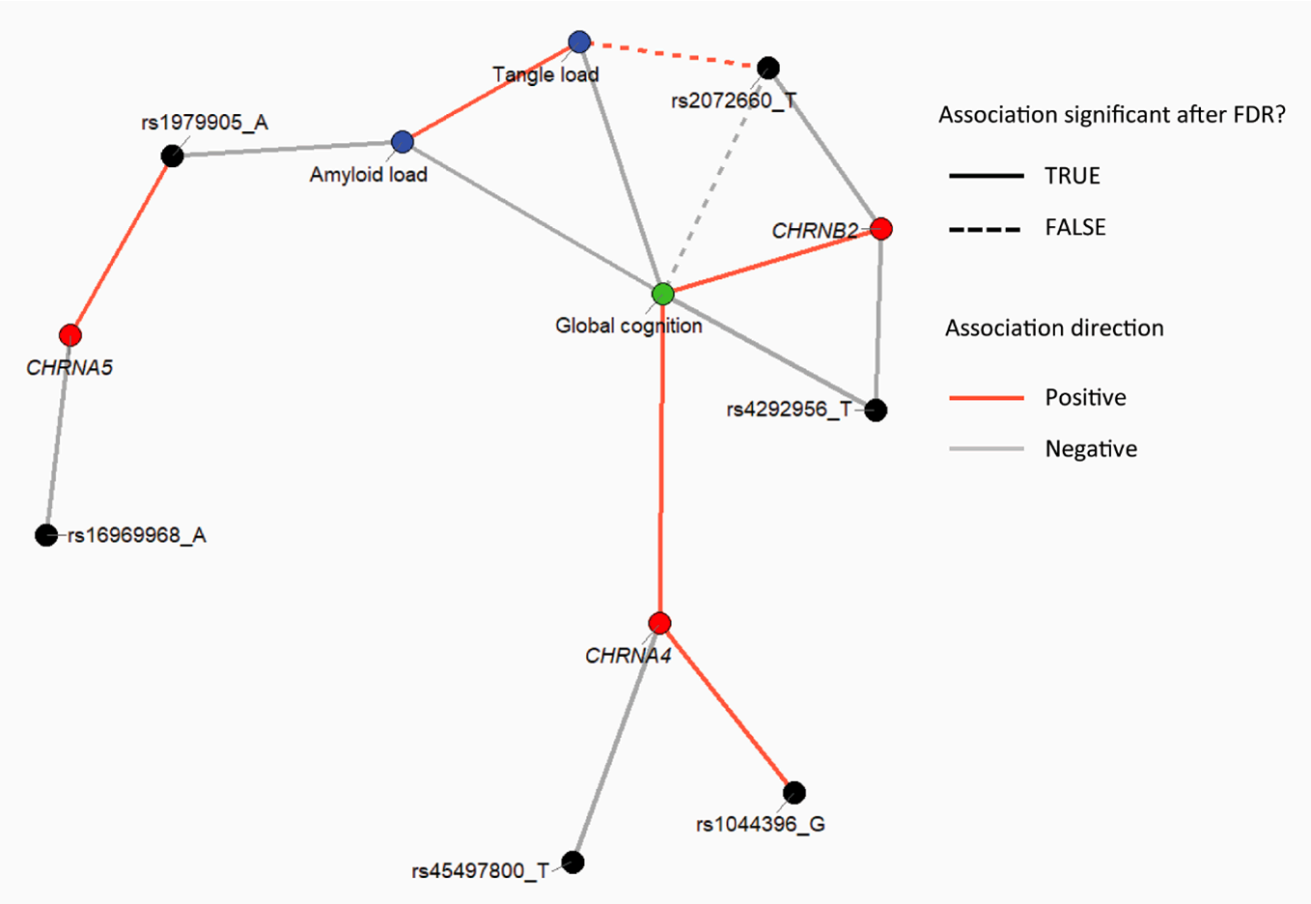
Tangle load
rs2072660_T
rs1979905_A
Amyloid load
CHRNB2
Global cognition
CHRNA5
rs4292956_T
rs16969968_A
CHRNA4
rs1044396_G
rs45497800_T
Association significant after FDR?
TRUE
FALSE
Association direction
Positive
Negative

Figure 2

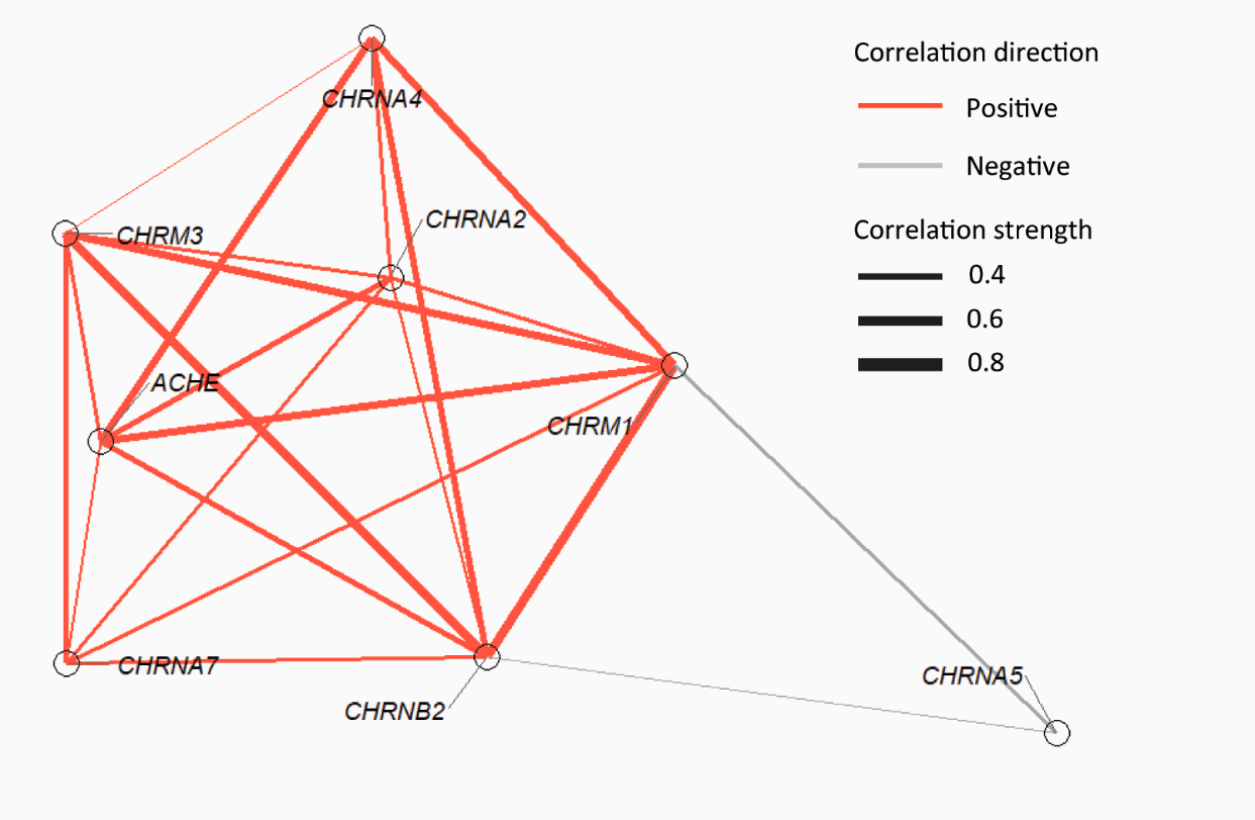
Correlation direction
Positive
Negative
Correlation strength
0.4
0.6
0.8
CHRNA4
CHRNA2
CHRM3
ACHE
CHRM1
CHRNA7
CHRNB2
CHRNA5

Figure 3

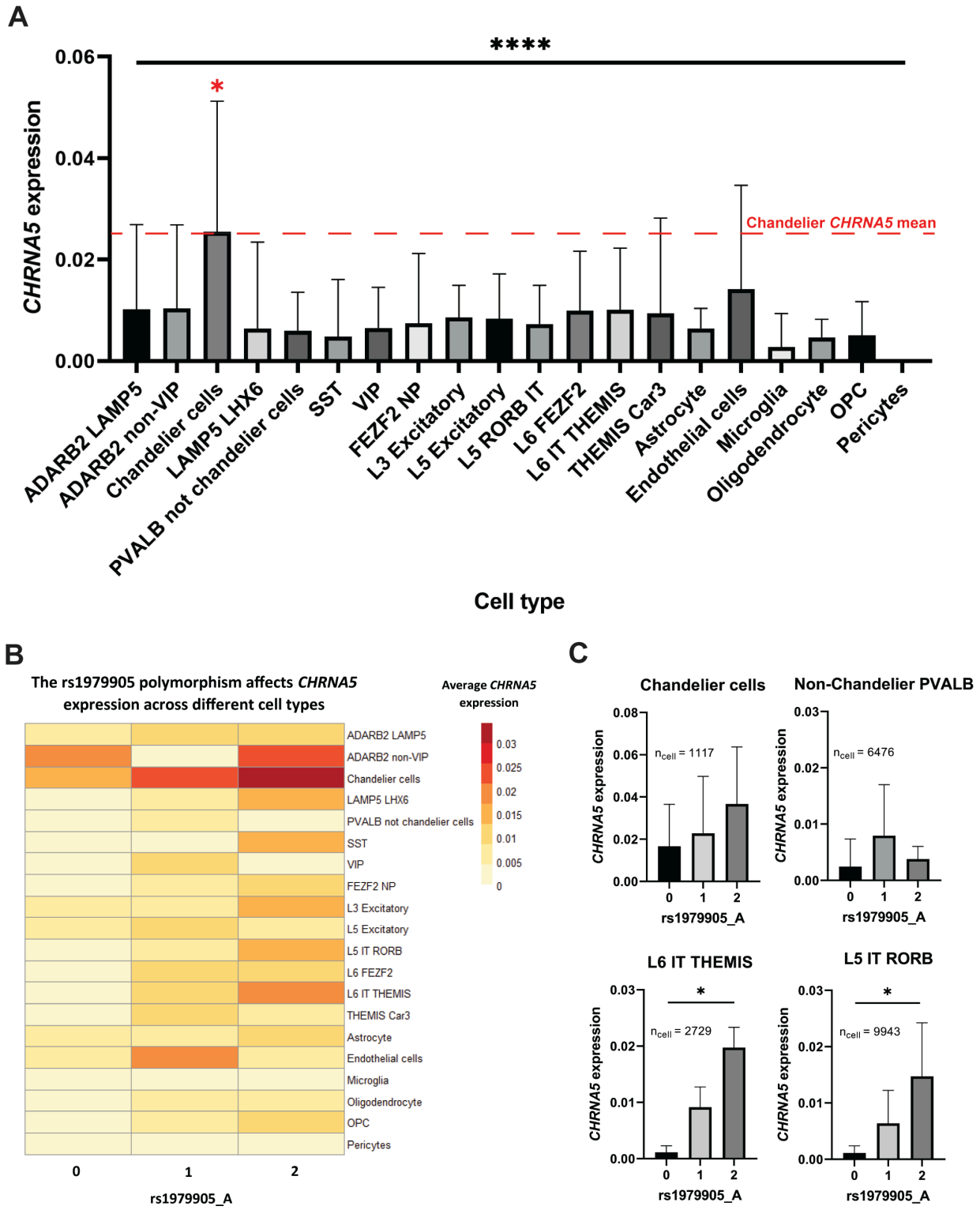
A
****
*
0.06
0.04
0.02
0.00
CHRNA5 expression
Chandelier CHRNA5 mean
ADARB2 LAMP5
ADARB2 non-VIP
Chandelier cells
LAMP5 LHX6
PVALB not chandelier cells
SST
VIP
FEZF2 NP
L3 Excitatory
L5 Excitatory
L5 RORB IT
L6 FEZF2
L6 IT THEMIS
THEMIS Car3
Astrocyte
Endothelial cells
Microglia
Oligodendrocyte
OPC
Pericytes
Cell type
B
The rs1979905 polymorphism affects CHRNA5 expression across different cell types
Average CHRNA5 expression
0.03
0.025
0.02
0.015
0.01
0.005
0
0
1
2
rs1979905_A
C
Chandelier cells
Non-Chandelier PVALB
L6 IT THEMIS
L5 IT RORB
n_cell = 1117
n_cell = 6476
n_cell = 2729
n_cell = 9943
CHRNA5 expression
rs1979905_A

Figure 4

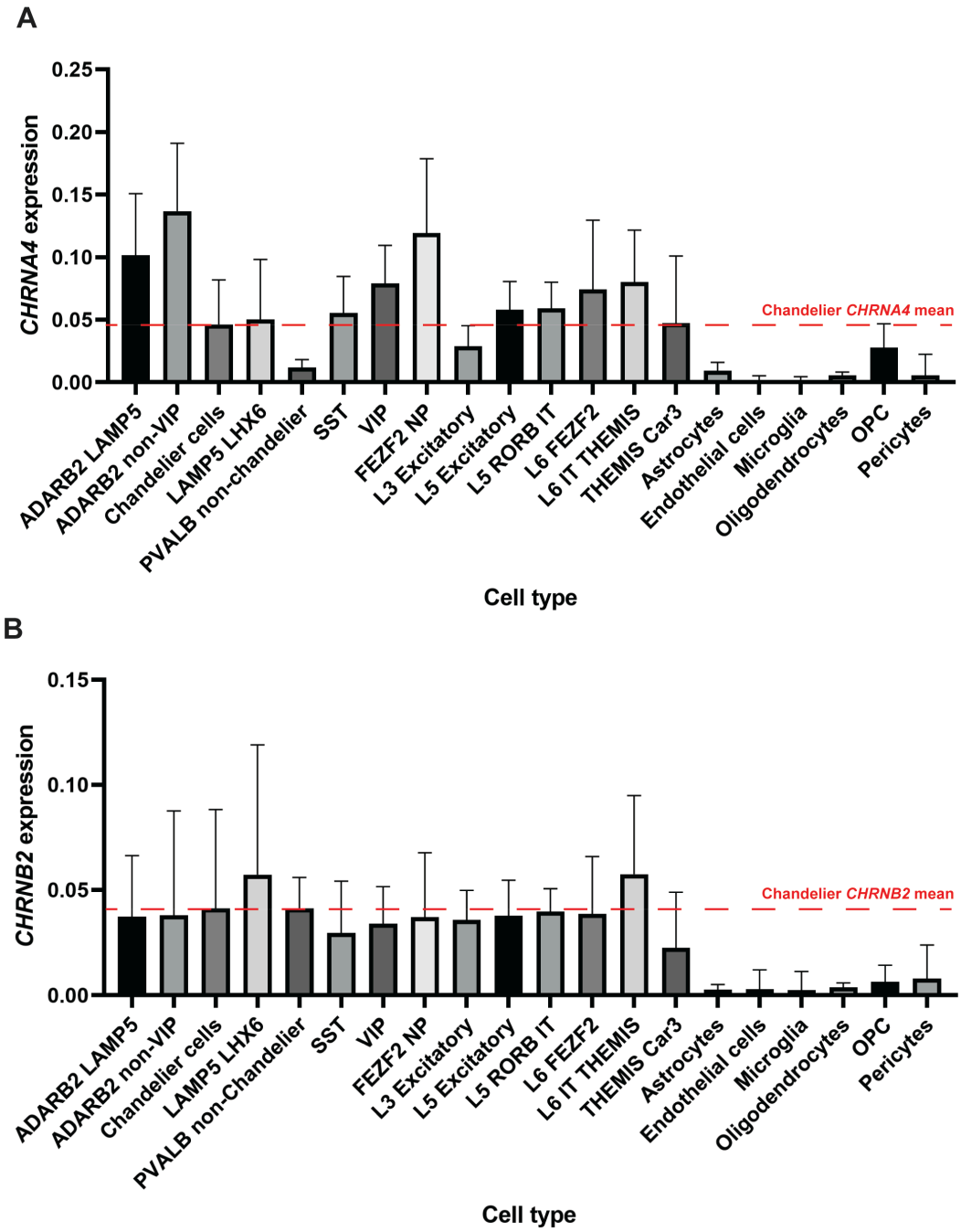
A
CHRNA4 expression
0.25
0.20
0.15
0.10
0.05
0.00
Chandelier CHRNA4 mean
ADARB2 LAMP5
ADARB2 non-VIP
Chandelier cells
LAMP5 LHX6
PVALB non-chandelier
SST
VIP
FEZF2 NP
L3 Excitatory
L5 Excitatory
L5 RORB IT
L6 FEZF2
L6 IT THEMIS
THEMIS Car3
Astrocytes
Endothelial cells
Microglia
Oligodendrocytes
OPC
Pericytes
Cell type
B
CHRNB2 expression
0.15
0.10
0.05
0.00
Chandelier CHRNB2 mean
ADARB2 LAMP5
ADARB2 non-VIP
Chandelier cells
LAMP5 LHX6
PVALB non-Chandelier
SST
VIP
FEZF2 NP
L3 Excitatory
L5 Excitatory
L5 RORB IT
L6 FEZF2
L6 IT THEMIS
THEMIS Car3
Astrocytes
Endothelial cells
Microglia
Oligodendrocytes
OPC
Pericytes
Cell type

Figure 5

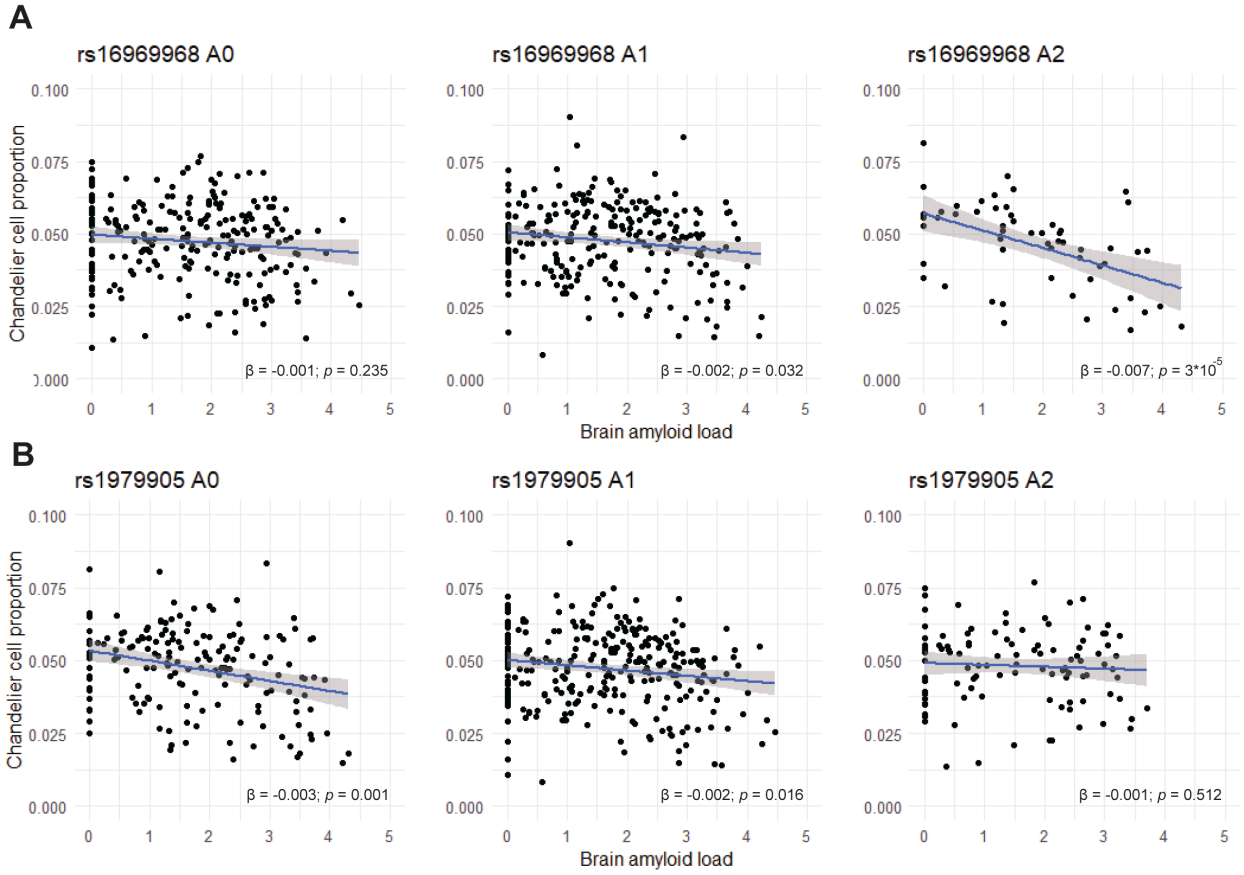
A
rs16969968 A0
rs16969968 A1
rs16969968 A2
Chandelier cell proportion
β = -0.001; p = 0.235
β = -0.002; p = 0.032
β = -0.007; p = 3*10^-5
Brain amyloid load
B
rs1979905 A0
rs1979905 A1
rs1979905 A2
Chandelier cell proportion
β = -0.003; p = 0.001
β = -0.002; p = 0.016
β = -0.001; p = 0.512
Brain amyloid load

Figure 6

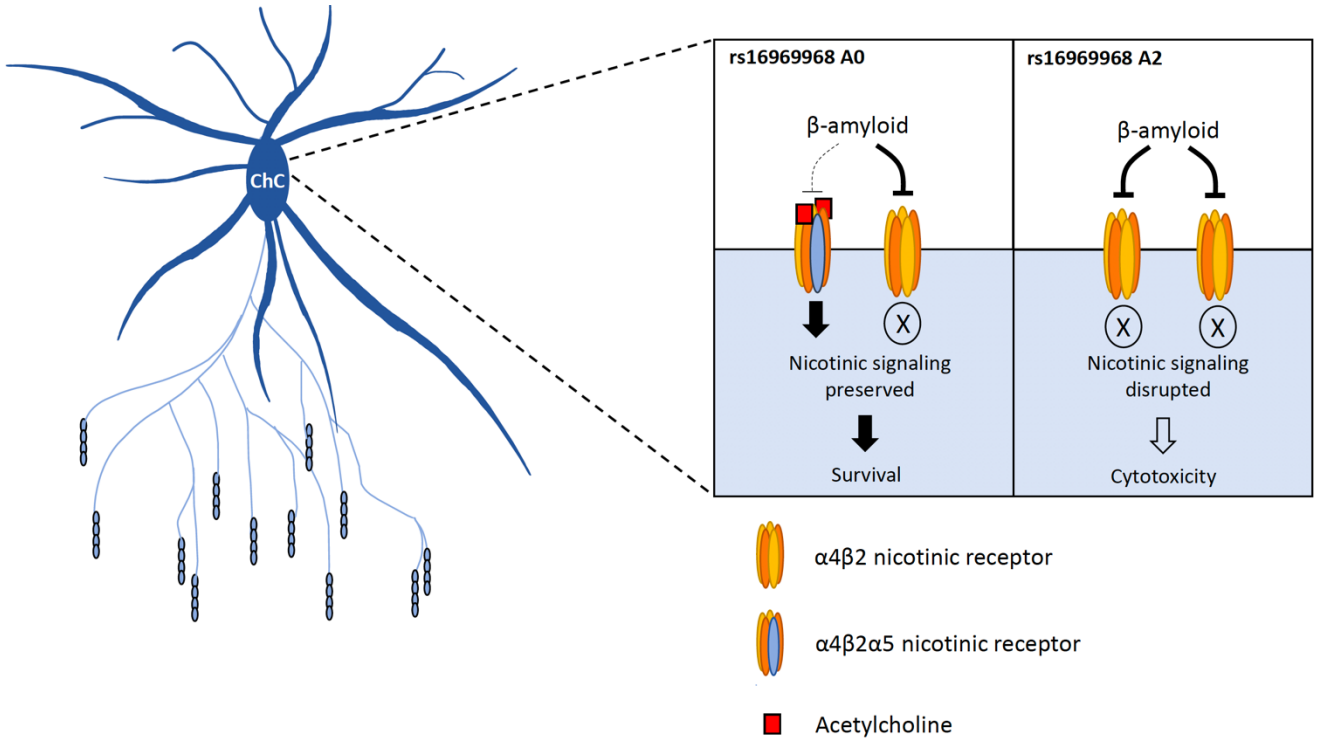
ChC
rs16969968 A0
β-amyloid
Nicotinic signaling preserved
Survival
rs16969968 A2
β-amyloid
Nicotinic signaling disrupted
Cytotoxicity
α4β2 nicotinic receptor
α4β2α5 nicotinic receptor
Acetylcholine

Figure 7